

Real-world observations of ~~reduced nitrogen and ultrafine particles~~ in commercial cooking organic aerosol emissions

Sunhye Kim¹, Jo Machesky², Drew R. Gentner², Albert A. Presto¹

¹. Department of Mechanical Engineering and Center for Atmospheric Particle Studies, Carnegie Mellon University, Pittsburgh, Pennsylvania, United States

². Department of Chemical & Environmental Engineering, Yale University, New Haven, Connecticut 06511, United States

Correspondence: Albert A. Presto (apresto@andrew.cmu.edu)

Abstract

Cooking is an important but understudied source of urban anthropogenic fine particulate matter (PM_{2.5}). Using a mobile laboratory, we measured PM size and composition in urban restaurant plumes. Size distribution measurements indicate that restaurants are a source of urban ultrafine particles (UFPs, particles <100 nm mobility diameter), with a mode diameter <50 nm across sampled restaurants and particle number concentrations (PNC, a proxy for UFPs) that were substantially elevated relative to the urban background. In our observations, PM mass emitted from restaurants was almost entirely organic aerosol (OA). Aerosol mass spectra show that while emissions from most restaurants were similar, there were key mass spectral differences. All restaurants emit OA at m/z 41, 43, and 55, though the composition (e.g., the ratio of oxygenated to reduced ions at specific m/z) varied across locations. All restaurant emissions included reduced nitrogen species detected as C_xH_yN⁺ fragments, making up ~15% of OA mass measured in plumes, with reduced molecular functionalities (e.g., amines, imides) that were often accompanied by oxygen-containing functional groups. The largest reduced nitrogen emissions were observed from a commercial bread bakery (i.e., 30-50% of OA mass), highlighting the

Deleted: ultrafine particles and reduced nitrogen

Formatted: Font color: Red

Formatted: Font color: Red

Deleted: The majority of observed PM was organic aerosol (OA) by mass.

30 marked differences between restaurants and their importance for emissions of both urban UFPs
31 and reduced nitrogen.

Deleted:

33 Introduction

34 Concentrations of most air pollutants, including fine particulate matter (PM_{2.5}) and
35 ultrafine particles (UFPs; particles with diameter <100 nm), are typically higher in urban areas
36 compared to rural or suburban areas (Cheng et al., 2019; Chow et al., 2006; Lenschow et al.,
37 2001; Louie et al., 2005; Renzi et al., 2021; Wang et al., 2020). Elevated urban concentrations
38 lead to higher human exposure, and in turn, contribute to the health impacts of air pollution.
39 PM_{2.5} exposures are associated with cardiovascular disease, lung cancer, and asthma and
40 contribute to up to 100,000 deaths annually in the US (Castillo et al., 2021). Although health
41 effects of UFP exposure are less extensively studied compared to PM_{2.5} (Schraufnagel, 2020) and
42 are an area of ongoing research, there is growing evidence that UFPs can enhance acute health
43 effects because of their small size and high surface area (Ali et al., 2022; Ibalid-Mulli et al., 2002;
44 Kwon et al., 2020).

45 The PM_{2.5} and UFP concentration enhancements in many urban areas are strongly
46 influenced by anthropogenic emissions (Apte et al., 2017; Li et al., 2018; Mohr et al., 2011; Saha
47 et al., 2019). Among a wide variety of contributing sources to air quality in the US, two notable
48 urban sources are mobile sources (e.g., motor vehicles) and cooking. These two sources
49 contribute to urban enhancements relative to the non-urban areas and to intra-urban spatial
50 variations in PM_{2.5} and UFP concentrations (Klompaker et al., 2015). In prior work, mobile
51 sources and cooking emissions have led to neighborhood-scale enhancements of ~0.5-1 µg m⁻³ of

Deleted: Among a wide variety of contributing sources,

Formatted: Font color: Red

54 PM_{2.5} in North American cities and a factor of two enhancement in UFPs (Rose Eilenberg et al.,
55 2020; Song et al., 2021b).

56 Motor vehicle emissions are well studied and have seen dramatic reductions as a result of
57 effective regulations on PM emissions across Europe and the US (Font et al., 2019; Keuken et
58 al., 2012). In contrast, there has been less attention to cooking sources as contributors of PM and
59 UFP emissions. As such, there have been fewer direct measurements and regulations dedicated
60 to cooking-related emissions, including everyday sources such as restaurants and home kitchens.
61 For comparison, two studies conducted in Pasadena, California revealed that organic PM_{2.5}
62 attributed to cooking decreased from approximately 2.4 µg/m³ to 1.2 µg/m³ between 1982 and
63 2010, while the contribution from traffic sources dropped from about 6.8 µg/m³ to 0.82 µg/m³
64 (Hayes et al., 2013; Schauer et al., 1996). This means that while total PM_{2.5} and vehicular-related
65 primary PM_{2.5} have decreased, the fraction of urban PM_{2.5} attributed to cooking has increased.

66 Aerosol mass spectrometry (AMS) measurements worldwide further indicate the
67 importance of cooking PM. Factor analysis utilizing PMF (Positive Matrix Factorization) on
68 AMS data routinely identifies a Cooking Organic Aerosol (COA) factor that represents between
69 6 - 25% of the total organic aerosol (OA) within PM₁ in urban settings. Specifically, a study in
70 Athens and Patras, Greece, showed that the COA contribution increased to 75% of organic PM₁
71 during mealtime in Patras (Florou et al., 2017). While the COA factor is routinely identified,
72 there can be significant variation in its composition from city to city (Bozzetti et al., 2017;
73 Crippa, El Haddad, et al., 2013; R. Hu et al., 2021; X.-F. Huang et al., 2010; Lee et al., 2015;
74 N. Pandis et al., 2016; Sun et al., 2012).

75 Many potential factors could produce variability in the composition and size distribution
76 of cooking PM. While the UFPs from cooking can contribute to ~ 80% of the total particle

Deleted: Factor analysis of AMS using PMF (Positive Matrix Factorization) data routinely identifies a Cooking Organic Aerosol (COA) factor that accounts for 6 - 25% of the total organic aerosol (OA) in urban environments.

Deleted: measurement

Commented [AP1]: Remove the Rogge paper from this list. It is not an AMS paper.

Deleted: (Bozzetti et al., 2017; Crippa, El Haddad, et al., 2013; R. Hu et al., 2021; X.-F. Huang et al., 2010; Lee et al., 2015; N. Pandis et al., 2016; Rogge et al., 1991a; Sun et al., 2012).

86 number concentrations indoors (Wan et al., 2011), there are a lot of factors—such as indoor-
87 outdoor air exchange rates (Wallace et al., 2004) and types of cooking oils used (Torkmahalleh
88 et al., 2012)—that can determine the size distribution of particles as well as the PM_{2.5}
89 concentrations from cooking activities. There is some evidence that the chemical composition of
90 cooking emissions may vary with the cooking style and the food cooked (Omelekhina et al.,
91 2020; Reyes-Villegas et al., 2018a; Takhar et al., 2019). For example, the cooking temperature,
92 ingredients, and methods used can alter chemical pathways that lead to the generation of
93 nitrogen-containing functional groups, including amides, within COA (Ditto et al., 2022).
94 Multiple studies found that nitrogen-containing composition has been observed while
95 charbroiling (Rogge et al., 1991a) or deep-frying hamburgers (Reyes-Villegas et al., 2018b;
96 Rogge et al., 1991a). Masoud et al., (2022) found that nitrogen-containing compounds
97 contributed 12-19% of the signal measured by a chemical ionization mass spectrometer for
98 emissions from typical in-home cooking. Overall, this variability across diverse cooking styles
99 and conditions is relevant but poorly understood. This implies a significant need for real-world
100 measurements to characterize and understand particle size and composition of cooking emissions
101 in urban environments.

102 This study aimed to characterize cooking emissions from real-world restaurant sources in
103 the US. We used a mobile laboratory to measure cooking emissions from nine restaurants in
104 Pittsburgh, PA and Baltimore, MD. Four of these restaurants were visited twice, making for a
105 total of thirteen cooking sites. Several analytical instruments, including an AMS and FMPS (Fast
106 Mobility Particle Sizer), were used at each site for online measurements, with supplemental PM
107 collection on Teflon filters for offline analysis. The measurements are used to examine variations
108 in UFP concentrations and cooking OA composition measured outside of restaurants with a

focus on contributions from reduced nitrogen components across restaurant sites visited during the field campaign.

2. Methods

2.1 Measurement locations

Table 1. Summary of restaurant locations and concentration enhancements measured in the cooking emission plumes over the entire sampling duration. Several restaurants were sampled on two separate days, as indicated by the number following the restaurant identifier. AMS high-resolution analysis of mean OA enhancement (CE=1), mean BC enhancement from aethalometer, Mode D_p (nm) measured by the FMPS, mean f₄₁ (the fraction of mass-to-charge ratio at 41 to the total organic mass signal), f₄₃, and f₅₅.

	City	Mean Δ OA (μg/m ³)	Mean Δ BC (μg/m ³)	Mean O:C ratio	Mode D _p (nm)	f ₄₁	f ₄₃	f ₅₅
<u>Island Cuisine</u>	<u>Pittsburgh</u>	<u>65</u>	<u>0.83</u>	<u>0.24</u>	<u>17</u>	<u>0.066</u>	<u>0.052</u>	<u>0.091</u>
<u>Pizza</u>	<u>Pittsburgh</u>	<u>100</u>	<u>3.2</u>	<u>0.18</u>	<u>29</u>	<u>0.066</u>	<u>0.056</u>	<u>0.092</u>
<u>BBQ</u>	<u>Baltimore</u>	<u>1.2</u>	<u>0.38</u>	<u>0.26</u>	<u>11</u>	<u>0.059</u>	<u>0.056</u>	<u>0.067</u>
<u>Café</u>	<u>Baltimore</u>	<u>2.3</u>	<u>0.35</u>	<u>0.40</u>	<u>8.1</u>	<u>0.043</u>	<u>0.081</u>	<u>0.043</u>
<u>Beef</u>	<u>Baltimore</u>	<u>15</u>	<u>4.2</u>	<u>0.34</u>	<u>11</u>	<u>0.081</u>	<u>0.072</u>	<u>0.10</u>
<u>Diner 1</u>	<u>Pittsburgh</u>	<u>77</u>	<u>1.4</u>	<u>0.24</u>	<u>11</u>	<u>0.064</u>	<u>0.044</u>	<u>0.076</u>
<u>Diner 2</u>	<u>Pittsburgh</u>	<u>84</u>	<u>2.0</u>	<u>0.12</u>	<u>11</u>	<u>0.075</u>	<u>0.052</u>	<u>0.089</u>
<u>Bakery 1</u>	<u>Baltimore</u>	<u>12</u>	<u>0.091</u>	<u>0.33</u>	<u>8.1</u>	<u>0.011</u>	<u>0.023</u>	<u>0.009</u>
<u>Bakery 2</u>	<u>Baltimore</u>	<u>4.6</u>	<u>0.41</u>	<u>0.29</u>	<u>8.1</u>	<u>0.023</u>	<u>0.047</u>	<u>0.020</u>
<u>Fast Food 1</u>	<u>Baltimore</u>	<u>1.7</u>	<u>1.4</u>	<u>0.39</u>	<u>29</u>	<u>0.029</u>	<u>0.062</u>	<u>0.023</u>
<u>Fast Food 2</u>	<u>Baltimore</u>	<u>3.8</u>	<u>0.36</u>	<u>0.29</u>	<u>11</u>	<u>0.053</u>	<u>0.065</u>	<u>0.055</u>
<u>Bar/Restaurant 1</u>	<u>Baltimore</u>	<u>69</u>	<u>2.4</u>	<u>0.28</u>	<u>11</u>	<u>0.085</u>	<u>0.065</u>	<u>0.099</u>
<u>Bar/Restaurant 2</u>	<u>Baltimore</u>	<u>140</u>	<u>5.0</u>	<u>0.30</u>	<u>26</u>	<u>0.075</u>	<u>0.075</u>	<u>0.12</u>

Field samples were collected from 13 visits to 9 urban cooking sites in Pittsburgh and Baltimore during July and August 2019 (Table 1). Candidate restaurants were identified using Google maps. We first identified an initial list of candidate restaurants by searching Google maps for restaurants located adjacent to a public road that seemed to have a horizontal exhaust vent pointed towards the road (Figure S1). We then visited each candidate restaurant location in

Moved (insertion) [1]

Deleted: ¶
City

Moved up [1]: ¶
City

Deleted: ¶
City

person to determine whether our mobile laboratory could be parked near the restaurant exhaust for emissions sampling.

Table 1 indicates the type of cuisine prepared at each restaurant. We tried to sample across a range of cuisines and price points. For example, one sampling location was a major fast-food chain that primarily serves hamburgers (Fast Food 1 and 2). Another location (Bar/Restaurant 1 and 2) was a more expensive restaurant where many entrees cost more than \$30. Lastly, we sampled twice outside of a large commercial bread bakery (Bakery 1 and 2).

Our procedure for identifying candidate restaurants has two important implications for our results. First, it means that the set of sampled restaurants represents a convenience sample and may therefore not be completely representative of the types of restaurants found in Pittsburgh or Baltimore. Second, since we did not coordinate with restaurant owners or operators during our sampling, we do not have detailed information about cooking fuel (though we assume that most restaurants used either gas or electricity), the specific cooking methods used, or the volume of food cooked during our sampling periods.

At each location, we parked a mobile laboratory near the restaurant's exhaust plume (SI Fig. 1). The selected restaurants represent a mix of accessible locations with visible emission plumes or exhaust vents. The sampling inlet on the mobile laboratory was typically within a few meters of the exhaust vent. However, this distance varied due to several uncontrollable external factors, such as the availability of parking and the height of the restaurants' exhaust vents. As a result, the measured emission plumes went through varying degrees of dilution before reaching our sampling inlet. At all locations we measured a mixture of fresh emissions and the ambient background air, though the fresh emissions were dominant. Nonetheless, it is important to

154 recognize that some of the variability we observe between restaurants could be the result of
155 dilution-driven changes in UFP and OA concentrations.

Deleted: As a result, the measured emission plumes went through varying degrees of dilution before reaching our sampling inlet.

156 Several of the restaurants were sampled on multiple visits to examine day-to-day
157 variations in emissions. These variations could be due to differences in activity (e.g., how many
158 customers ordered food), the type of food ordered, and differences in dilution conditions. Each
159 visit to a restaurant site lasted approximately 30-60 minutes. The sampling periods targeted
160 expected times for lunch (~11 am – 1 pm) and dinner (~6 – 8 pm).

162 *2.2 Mobile laboratory and measurements*

163 Instruments were loaded into a gasoline-powered mobile laboratory. At each location, we
164 oriented the mobile laboratory so that the vehicle exhaust was located downwind of the sample
165 inlet to minimize self-contamination from the vehicle exhaust.

166 We use total particle number concentration (PNC) as our proxy for UFPs. Particle
167 number counts were measured by a MAGIC™ water CPC (Moderated Aerosol Growth with
168 Internal water Cycling Condensation Particle Counter, Aerosol Devices Inc, Model
169 MAGIC200P). MAGIC CPC uses water condensation to enlarge particles through a 3-
170 temperature stage growth tube. The enlarged particles are counted with a laser sensor up to
171 400,000 particles cm⁻³ with a particle size range between 5 nm and 2.5 μm in diameter (Hering et
172 al., 2019). Saha et al., (2019) previously observed that the MAGIC CPC undercounts relative to a
173 butanol CPC. Thus, the raw CPC output was adjusted using a correction factor determined from
174 the co-location of the MAGIC CPC with a TSI 3772 butanol CPC.

175 Particle size distributions and total number concentrations were measured with FMPS
176 (Fast Mobility Particle Sizer, TSI Inc, Model 3091) for particles with diameters from 6.04 nm to

180 523.3 nm. The FMPS reported systematically lower particle counts than the MAGIC CPC (factor
181 of 3.5, SI Section 2 and Fig. S2). FMPS data were utilized in lieu of the CPC data due to high
182 particle number concentrations in restaurant plumes that exceeded the upper counting limit of the
183 CPC (400,000 particles cm^{-3}), resulting in error flags. To ensure consistency with the MAGIC
184 CPC, all FMPS data were corrected by integrating the FMPS size distribution, which was scaled
185 by the FMPS:CPC ratio.

186 A High-Resolution AMS (HR-AMS, Aerodyne), which measures non-refractory particles
187 with a diameter less than 1 μm (NR-PM₁), was used to identify mass spectra of PM components
188 (Organics, NH_4^+ , NO_3^- , SO_4^{2-} , and Cl^-) in real-time. Squirrel (SeQUential Igor data RetTriEvaL)
189 toolkit 1.62G and Pika (Peak Integration by Key Analysis) toolkit 1.22G in Igor Pro
190 (Wavemetrics, Lake Oswego) were used for the HR-AMS data analysis. For the baseline and
191 peak fitting correction procedures of the HR-AMS data, the high-resolution range of m/z (mass-
192 to-charge ratios) 12 to 140 was selected. All AMS analysis presented here assumes a collection
193 efficiency (CE) of one.

194 An aethalometer (Magee Scientific, Model AE33), CO analyzer (Teledyne API T300),
195 and CO₂ analyzer (LiCor LI-820, Biosciences) measured black carbon (BC), CO, and CO₂
196 concentration, respectively.

197 PM_{2.5} samples were collected at ~70 L/min on 47 mm PTFE membrane filters (47 mm,
198 2.0 μm pores, Tisch Scientific) through a separate inlet mounted close to the online
199 instrumentation inlet outfitted with a cyclone (2.5 μm cut point with a flow rate of 92 LPM,
200 URG-2000-30EH, URG cyclone). At each restaurant site where plumes were observed via AMS,
201 a filter sample was collected for at least 30 minutes and Table S3 shows details for each filter
202 sample. Filter samples were transported on ice packs from the mobile lab and kept in sample

storage freezers. Additional filter collection details can be found in the Supporting Information. All samples were analyzed via liquid chromatography (LC) using an Agilent Infinity LC and an Agilent Poroshell 120 SB-Aq reverse-phase column (2.1×50 mm, 2.7 µm particle size). The LC was coupled to an electrospray ionization (ESI) source, operated in positive and negative modes for each sample, and connected to a high-resolution mass spectrometer (Agilent 6550 Q-TOF). These instruments were operated following previously described methods (Ditto et al., 2018, 2020).

Selected samples showing unique AMS spectra with nitrogen-containing compounds underwent further analysis via MS/MS (tandem mass spectrometry) with the objective of identifying the distribution of functional groups within the reduced nitrogen species that were observed via LC-TOF, similar to prior work (Ditto et al., 2020, 2022). LC-TOF mode data processing and QC/QA have previously been described (Ditto et al., 2018), and details of compound selection for MS/MS analysis in this study can be found in the Supporting Information (Section S3). MS/MS spectra analysis used SIRIUS with CSI:FingerID for molecular structure prediction (Dührkop et al., 2015, 2019), and the APRL Substructure Search Program was used for functional group identification from the predicted SMILES formula for atmospherically-relevant groups (Ruggeri & Takahama, 2016). Further details on LC-MS/MS analysis, processing, and associated limitations of ESI and MS/MS spectra analysis can be found in Ditto et al., (2020), with brief comments on relevant SIRIUS updates in the Supporting Information (Section S3).

3. Results and Discussion

3.1 Typical measurements of restaurant emission

Figure 1 demonstrates observations collected during a typical sampling day via the mobile lab in Baltimore. On this day, the mobile laboratory was initially (~15:36 – 16:49 EDT) parked in an urban park, here noted as background. Sampling was then conducted on-road, driving on various streets in urban Baltimore, from 16:49 to 18:20. At 18:20; the mobile laboratory was parked outside a restaurant (Bar/Restaurant 2).

The data in Figure 1 exemplify clear variations in pollutant concentrations between the background, on-road, and restaurant portions of sampling. In general, concentrations were the lowest and least variable in urban background locations and the highest and most variable for the restaurant sampling periods.

Nearby vehicles significantly impacted the measured concentrations during the on-road sampling period, thus differentiating it from the background period, where direct observations of on-road emissions were minimal. Concentrations of CO, CO₂ (Fig. 1a), organic aerosol (OA), black carbon (BC, Fig. 1b), and particle number (Fig. 1d) were all elevated in the on-road samples compared to the urban background.

In order to quantify concentrations differences between microenvironments (e.g., on-road versus background), we compute the enhancement of all species above the urban background (e.g., Δ OA). We did this by defining the background concentration as the 5th percentile of measurements made in the background location on each sampling day. This background concentration is then subtracted from the measurements to determine local concentration enhancements. Background concentrations for BC and OA are listed in Table S1 of the SI. While many other background correction methods have been proposed in the literature (Actkinson et

Deleted: likely

Formatted: Font color: Red

Commented [AP2]: cite this paper:
<https://amt.copernicus.org/articles/14/5809/2021/>

al., 2021), the overall results presented in Figure 1 are not sensitive to our specific choice of background correction method.

The mean organic aerosol concentrations are $5.8 \mu\text{g}/\text{m}^3$ (ΔOA : $2.46 \mu\text{g}/\text{m}^3$) during on-road sampling versus $4.2 \mu\text{g}/\text{m}^3$ (ΔOA : $0.85 \mu\text{g}/\text{m}^3$) in the urban background (Fig. 1b). Similarly, the BC concentration was $0.5 \mu\text{g}/\text{m}^3$ higher on-road than in the urban background, and PNC was approximately a factor of three higher on-road than in the urban background. These enhancements in organic aerosol, black carbon, and PNC are broadly consistent with enhancements with those seen in high-traffic areas by our previous sampling in Pittsburgh and Oakland (Saha et al., 2020; Shah et al., 2018).

In addition to the overall increase in pollutant concentrations on-road, there are occasional, coincident spikes in CO, BC, OA, and PNC during the on-road sampling. The particle size distribution also changes during these spikes (Fig. 1c), with higher concentrations of particles in the 20-100 nm size range. These are likely plumes from nearby high-emitting vehicles, potentially diesel trucks and buses (Dallmann et al., 2013; Tan et al., 2016).

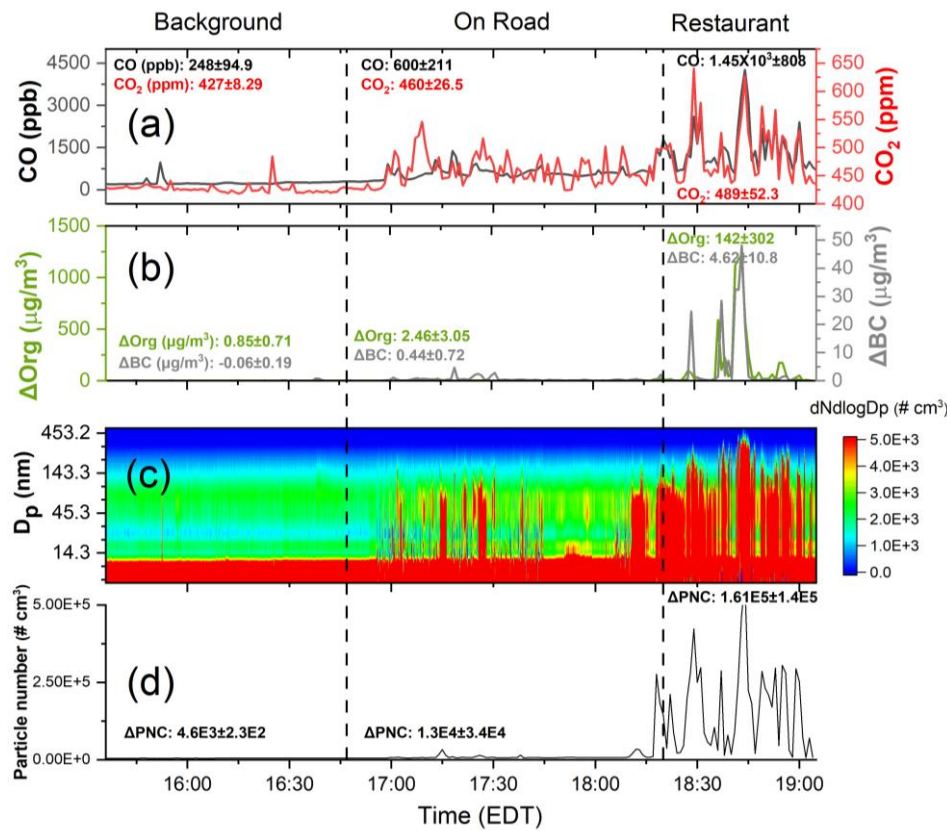
The highest and most variable concentrations are observed in the restaurant plume. In this near-source environment, organic aerosol concentrations averaged $146 \mu\text{g}/\text{m}^3$. This is 35 times higher than the urban OA background. Particle number counts were also 35 times higher in concentration than background levels. CO, CO₂, and BC enhancements were also observed when the mobile lab was parked near the restaurant. The enhancement of CO was 5.9 times the background, CO₂ and BC were 1.15 and 5.42 times higher, respectively.

During the restaurant sampling period, there are several clear and concurrent spikes in OA (Fig. 1b) and particle number count (Fig. 1d). These seem to be associated with specific events, such as preparing a customer's new order (restaurant kitchens had varying activity levels

Formatted: Font color: Red

Deleted: ΔOA and ΔBC were calculated by subtracting the background concentration from the measured OA or BC mass concentration. The background concentration is defined as the 5th percentile of data collected on each sampling day (listed in Table S1).¶

278 during the sampling periods). The size distributions in Figure 1c show that these emissions span
 279 a wide range in particle size, from <10 nm up to a few hundred nm, demonstrating that
 280 restaurants may be a source of urban ultrafine particles.
 281



282
 283
 284 **Figure 1.** Urban background, on-road, and restaurant plumes observed during a typical sampling
 285 day (Bar/Restaurant 2) in Baltimore, showing: (a) CO and CO₂, (b) background corrected
 286 organic aerosol (OA) and black carbon (BC) concentrations, (c) particle size distribution from
 287 FMPS, and (d) background-corrected total particle number concentrations. All concentrations
 288 were significantly higher and more variable in restaurant emissions plume than in the urban
 289 background or on-road period. Numbers in (a), (b), and (d) indicate the mean ± standard
 290 deviation for each sampling period.

291
292 While average BC concentrations were about a factor of five higher than background
293 during the restaurant sampling period, BC seems to be a relatively smaller component of PM
294 emissions from the restaurant. The OA/BC ratio in the urban background and on-road sampling
295 periods was ~4. In the restaurant plume, the mean OA/BC ratio was 28. Despite occasional
296 periods of very high BC concentrations reaching up to 58 $\mu\text{g}/\text{m}^3$, the OA/BC ratio during the
297 spike was 230 (Fig. S3). Other PM components (e.g., sulfate and nitrate) show no discernable
298 enhancement during the restaurant sampling period (Fig. S4). This indicates that the PM
299 emissions from the restaurant were dominated by organic aerosol.

300 We also observed elevated concentrations of CO and CO₂ in the restaurant exhaust. We
301 do not have information about each restaurant's cooking practices or fuels (i.e., whether the
302 restaurants used natural gas or electricity). Jung & Su (2020) showed that food cooking emits
303 CO, so the CO spikes observed here may also be from the food rather than fuel combustion.
304 Other recent measurements in Pittsburgh by (Song et al., 2021a) also showed enhancements in
305 CO during mealtimes in a restaurant-rich area.

306

307 3.2 Summary of organic aerosol enhancements at restaurant sites

308 Figure 1 shows the OA enhancement at a single restaurant. Enhancements in OA because
309 of emissions from restaurants were similarly observed across all other sampling sites that we
310 visited. Figure 2 is a box-plot visualization of the OA enhancement (ΔOA) for each restaurant
311 visit. The data are split into two main groups for visual clarity: high concentration (mean $\Delta\text{OA} >$
312 $50 \mu\text{g m}^{-3}$, Fig. 2a) and low concentration (mean $\Delta\text{OA} < 30 \mu\text{g m}^{-3}$, Fig. 2b). Because of the
313 variation in distance from the exhaust of each restaurant and our sampling inlet, the

Formatted: Font color: Red

Deleted: as a result

concentration enhancements shown in Figure 2 are the result of both the emissions from each restaurant and dilution of the emission plume before sampling.

Formatted: Font color: Red

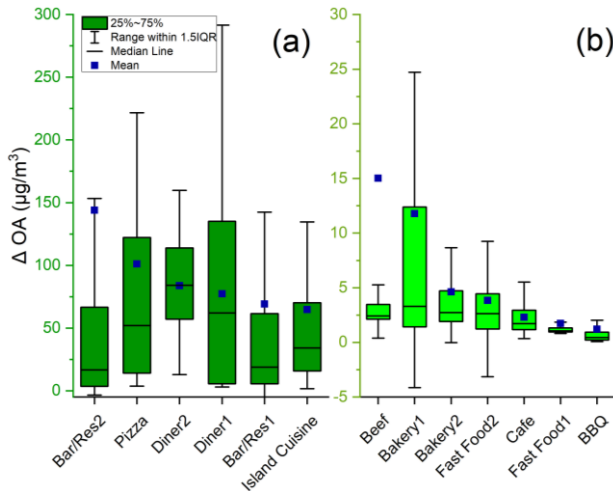


Figure 2. Organic aerosol enhancement (ΔOA) at each restaurant site with (a) high (mean $\Delta OA > 50 \mu g/m^3$) and (b) low (mean $\Delta OA < 30 \mu g/m^3$) enhancements grouped in each for comparison. The sample names in (a) and (b) are ordered by decreasing mean concentration.

There is significant variability in measured ΔOA between and within each restaurant (Fig. 2 and Fig. S4). For nearly every location sampled, the emissions varied over time, as shown in Figure 1, and this contributes to wide interquartile ranges (IQRs) in Figure 2. It also means that at nearly every restaurant, there were periods when the concentration was near the urban background level, as indicated by the whiskers reaching (or even going slightly below) zero.

The temporal variability of the concentrations measured at each restaurant contributed to an upward skew in ΔOA , with a mean concentration greater than the 75th percentile at many locations. This suggests that the measurements were dominated by short, intense bursts of emissions rather than sustained high concentrations. Visualizations of this trend are noticeable in

Figure 1b, where there is a large spike in emissions so that OA goes above 1000 $\mu\text{g}/\text{m}^3$ for several minutes. The temporal variability seems to be associated with the quantity of cooking that spikes amid busy mealtimes.

Four restaurants were sampled on multiple days (Bar/Restaurant, Fast Food, Bakery, and Diner). While there were day-to-day differences in the mean ΔOA at each location, each of these locations fell into the same group (i.e., $\Delta\text{OA} < 30 \mu\text{g m}^{-3}$ or $\Delta\text{OA} > 50 \mu\text{g m}^{-3}$) on both sampling days. This suggests that the day-to-day variations in emissions are smaller than within-day emissions for each location and that high-emitting restaurants are consistently high emitters. However, due to the limitation of a single visit to each sampling location during the campaign, it may be challenging to conclusively ascertain that the classification assigned to the sampled restaurants is not indicative of all similar cooking operations.

3.3 OA composition across restaurants

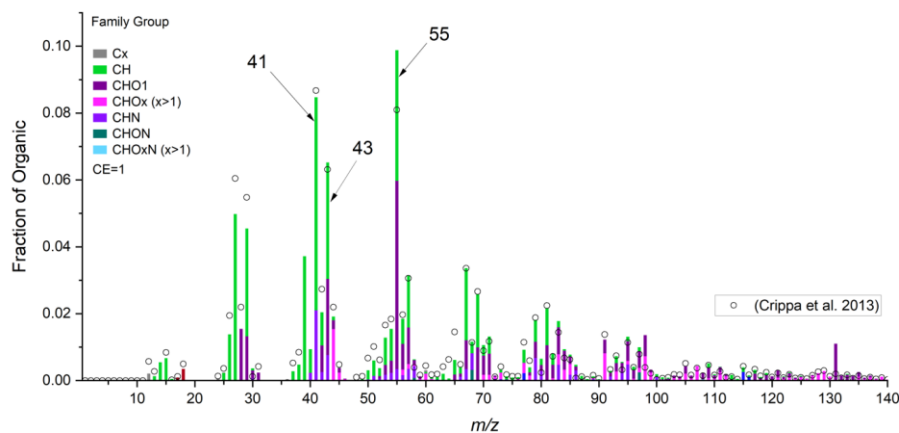


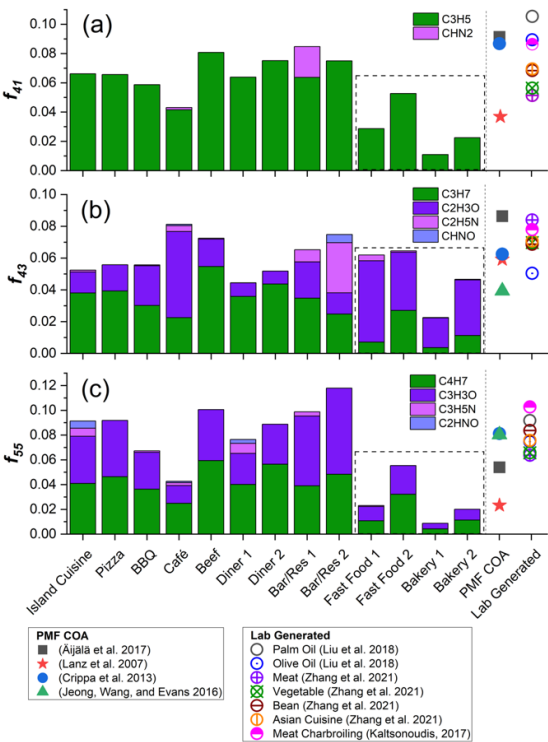
Figure 3. Mass spectrum from the entire sampling period at Bar/Restaurant 2 and comparison with the COA mass spectrum for Paris determined from PMF by Crippa et al. High-resolution

mass spectra are grouped into sticks of the unit mass resolution, which colors indicating mass fraction of chemical families.

In this section, we compare the composition of cooking OA across the restaurants and to previous laboratory measurements and ambient factor analysis. Figure 3 shows the mean mass spectrum of OA measured at Bar/Restaurant 1 in Baltimore; mass spectra from three additional restaurants are shown in Figure S5. The mass spectrum contains a mixture of hydrocarbon (C_xH_y) and oxygenated (C_xH_yO) ions. This is consistent with the composition of cooking OA, which is often dominated by long-chain fatty acids from heated cooking oils and from meat cooking (Crippa, DeCarlo, et al., 2013; D. D. Huang et al., 2021a; Liu et al., 2017; Mohr et al., 2009; Takhar et al., 2019; Z. Zhang et al., 2021). Several lab experiments from seed oil cooking detected fatty acids or degradation fragments such as *n*-alkanoic acid, *n*-alkenoic acid, oleic acid, and carbonyls (Allan et al., 2010; Liu et al., 2018; Schauer et al., 2002). Unlike oils, which are entirely comprised of fats, meats contain proteins and fats, although the composition can vary depending on the type of meat. Cooking meat generally emits cholesterol and fatty acids like palmitic acid, stearic acid, and oleic acid (Rogge et al., 1991a; Schauer et al., 1996), which have all been used as chemical markers of meat cooking emissions. This mixture of hydrocarbon and oxygenated ions is also identified in PMF factor analysis of ambient datasets, as indicated by the mass spectrum from Crippa, DeCarlo, et al., (2013) shown in Figure 3.

The most abundant peaks in the mass spectrum were at m/z 41 (mostly $C_3H_5^+$), 43 ($C_2H_3O^+$ and $C_3H_7^+$), and 55 ($C_3H_3O^+$ and $C_4H_7^+$). These peaks have been used as COA markers for tracing cooking sources in previous studies (Allan et al., 2010; Dall'Osto et al., 2015; Kaltsonoudis et al., 2017; Mohr et al., 2009). Table 1 summarizes the mean contribution (f_{41} , f_{43} , and f_{55}) at these m/z to each restaurant's overall OA mass spectrum.

Deleted: Figure 3. Example mass spectrum from Bar/Restaurant 1 in this study and comparison with the COA mass spectrum from prior PMF work. High-resolution mass spectra are grouped into sticks of the unit mass resolution, and the coloring of each stick represents the mass fraction belonging to different chemical families.¶



380

381 **Figure 4.** Fraction of (a) m/z 41, (b) 43, and (c) 55 to the total organic aerosol mass
382 concentrations and comparison to COA mass spectra from prior PMF studies (Äjjälä et al., 2017;
383 Crippa, DeCarlo, et al., 2013; Jeong et al., 2016; Lanz et al., 2007) and laboratory-generated
384 cooking emissions (Kaltsonoudis et al., 2017; Liu et al., 2018; Z. Zhang et al., 2021). Only f_{43}
385 and f_{55} were shown in (Jeong et al., 2016) (f_{41} was not provided in the paper). Fast Food and
386 Bakery samples are grouped in a box as they showed lower abundances of these common
387 cooking marker fractions (f_{41} , f_{43} , and f_{55}).
388

389 Figure 4 compares f_{41} (OA mass fraction at m/z 41), f_{43} , and f_{55} across the restaurants
390 sampled here to previously published COA mass spectra. We compared two types of previous
391 studies: COA mass spectra derived from factor analysis of ambient data using PMF and

laboratory measurements of cooking emissions. The laboratory measurements shown here include a combination of heating palm and olive oils (Liu et al., 2018) and various cooking experiments using meats (chicken and pork), vegetables, beans, and Asian cuisine (Kaltsonoudis et al., 2017; Z. Zhang et al., 2021).

For m/z 41, our data were dominated by the hydrocarbon ion ($C_3H_5^+$), which was approximately 4-8% of OA mass for most of the restaurants. The exceptions were Fast Food 1 and the two samples collected at the Bakery location. These had lower f_{41} (1-5%) and are shown inside the dashed box. f_{41} fractions from our study were generally lower than from the PMF COA factors. Three of the four COA factors have f_{41} of ~9% (Äijälä et al., 2017; Crippa, DeCarlo, et al., 2013; Jeong et al., 2016). The COA factor from Lanz et al., 2007 is 4% and is lower than most of the restaurants we sampled here. There is a wide range in f_{41} from the laboratory experiments. The two oil heating experiments (palm and olive oil, Liu et al., 2018) generated higher f_{41} than most of our measurements (8-10%). There was a wider range in f_{41} for food cooking experiments (5-8%), and there is a strong overlap with our measurements.

For f_{43} and f_{55} , both oxidized (e.g., $C_2H_3O^+$ and $C_3H_3O^+$) and hydrocarbon (e.g., $C_3H_7^+$ and $C_4H_7^+$) ion fragments showed significant contributions across the urban cooking sites. There were also minor contributions from nitrogen-containing ions (e.g., $C_2H_5N^+$ and C_2HNO^+). Except for Bakery 1, f_{43} was ~5-8% in our measurements. However, there was variation in the relative abundance of the hydrocarbon and oxygenated ions. For most sites, the contribution of the hydrocarbon ion ($C_3H_7^+$) was larger than the oxygenated ion ($C_2H_3O^+$). However, the sites with low f_{41} , Bakery and Fast Food 1, m/z 43 fragments were mostly oxygenated (mean = 3.5%).

The mean f_{43} in the PMF profiles was 6.3% with a range of 4-8.7%, which is similar to the mean and range observed in our dataset. Similarly, the laboratory emissions data cluster

Formatted: Font color: Red

415 around f_{43} of 8%, with slightly lower f_{43} in the heated oil experiments. This is slightly higher
416 than the f_{43} measured in the restaurant emissions.

417 The pattern in f_{55} is similar to f_{43} ; contributions are dominated by the hydrocarbon and
418 oxygenated ion, with minor contributions from N-containing ions. For most sites, including the
419 Bakery and Fast Food sites, the contributions of hydrocarbon and oxygenated ions at m/z 55 are
420 similar. The largest difference is that the Bakery and Fast Food sites have significantly lower f_{55}
421 (1-6%) than the other sites (4-12%). Additionally, for many of the sites, f_{55} is larger than the
422 PMF factors and the laboratory experiments.

423 The variations in f_{41} , f_{43} , and f_{55} , as well as variations in the ratios between these m/z s,
424 may indicate the food cooked at the different restaurants. For example, f_{41} appears to be larger
425 than f_{43} for cooking emissions from oil, as observed in the oil heating experiments by Liu et al.
426 (2018) and in laboratory oil cooking emissions by Allan et al. (2010). Meat cooking emissions
427 seem to have the opposite relationship, with $f_{43} > f_{41}$. Both oil cooking and meat cooking have
428 high f_{55} , and meat cooking may have $f_{55} > f_{43}$ (Mohr et al., 2009).

429 For most restaurants sampled here (except for both Bakery and Fast Food), m/z 55 is the
430 most abundant signal in the aerosol mass spectrum. Additionally, f_{41} is slightly higher than f_{43} for
431 these sites. This suggests a mixture of meat and oil cooking at these locations. For Bakery and
432 Fast Food, f_{43} is typically the most abundant ion, with f_{41} exceeding f_{55} . This may suggest a
433 different mix of food being cooked, or a difference in the cooking style, however, there is
434 insufficient evidence in the mass spectra to conclusively explain the differences.

Deleted: For example, f_{41} seems to be larger than f_{43} for cooking emissions dominated by oil; this is the case in the oil heating experiments from Liu et al. 2018 as well as from laboratory oil cooking emissions measured by Allan et al. (Allan et al., 2010).

Formatted: Font color: Red

Deleted: (except Bakery and Fast Food),

Formatted: Font color: Red

Formatted: Font color: Red

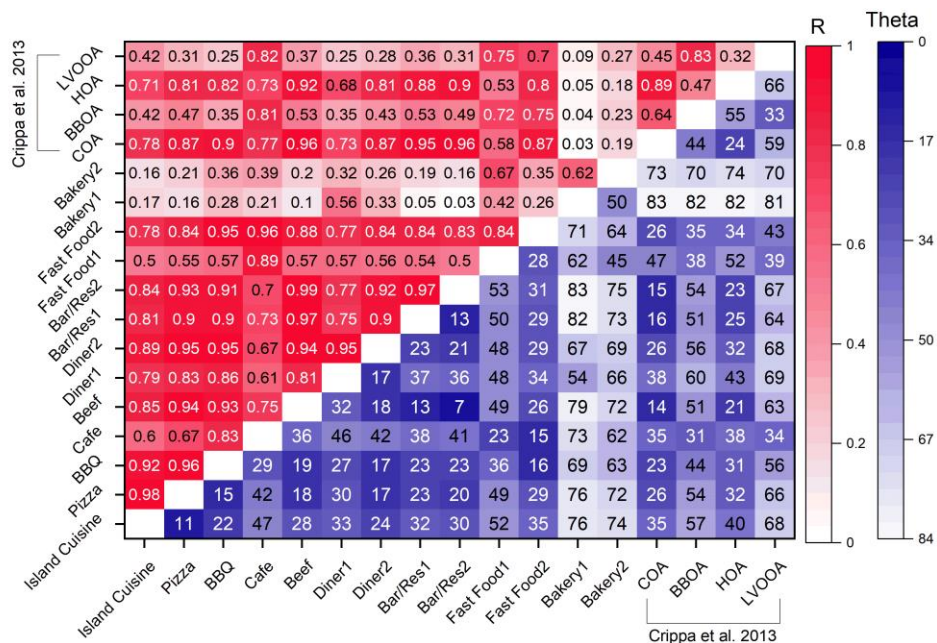


Figure 5. Comparison of the AMS UMR (unit mass resolution spectra) in two urban areas using correlation coefficients (R) and cosine similarity (θ , in degrees). R values close to 1 and θ values close to 0 mean strong correlations of mass spectra. Both R and θ values are presented such that darker colors correspond to higher similarity.

Figure 4 compares the cooking OA mass spectra for specific marker ions. Figure 5 compares the full cooking OA mass spectra. We use two metrics: the Pearson correlation (R) and cosine similarity. The statistical approach, correlation coefficient R, has been widely used in many studies, such as the analysis of air quality, to show an association between any two variables (Devarakonda et al., 2013; Giorio et al., 2012; Kiendler-Scharr et al., 2009; Raatikainen et al., 2010). Cosine similarity treats pairs of mass spectra as vectors and computes the angle (θ) between them (Kaltsonoudis et al., 2017; Kostenidou et al., 2009). θ is a measure of the similarities between two mass spectra, with a value of 0° , meaning that both spectra are

455 identical and $\theta > 30^\circ$ indicating considerable differences between the spectra. Cosine similarity is
456 more sensitive to smaller differences in mass spectra than R, as the correlation coefficient can be
457 dominated by ions with large abundance (Kaltsonoudis et al., 2017). Figure 5 also compares the
458 cooking emissions to PMF factors retrieved from Paris during winter (Crippa, DeCarlo, et al.,
459 2013) for biomass burning (BBOA), combustion emissions (HOA), and secondary OA
460 (LVOOA) obtained from the Jimenez Research Group website.
461 (<http://cires1.colorado.edu/jimenez-group/AMSsd/>).

462 Overall, the COA measured from most of the restaurants is similar. Of the 78 restaurant-
463 restaurant pairs, 33 have $R > 0.8$ and 49 have $\theta < 30^\circ$. These metrics underscore a notable
464 similarity in mass spectra across a significant proportion of the sampling sites. The exceptions
465 are the Bakery samples and, to a lesser extent, the Fast Food samples. These sites contribute the
466 majority of the cases where $R < 0.8$ and $\theta > 30^\circ$.

467 Bakery samples had $R < 0.3$ and $\theta > 50^\circ$ when compared to most of the other restaurants.
468 This suggests that the emissions from the bakery site were fundamentally different than
469 emissions from the other restaurants. While we do not have details on the specific activities at
470 the bakery on the two days when we sampled, the bakery clearly prepares different food than
471 many of the restaurants. For example, the bakery does not cook meat. The following section
472 discusses key mass spectral differences in more detail.

473 The other location where the mass spectrum was different from other restaurants was Fast
474 Food. There were day-to-day differences in the Fast Food mass spectrum, with one day (Fast
475 Food 1) being similar to other restaurants ($R = 0.7-0.8$, $\theta < 30^\circ$), and the other day (Fast Food 2)
476 having lower R and higher θ .

Deleted: For most restaurants, the R between mass spectra is larger than 0.8 and θ is less than 27° , suggesting that the mass spectra are similar. Figures 3 and 4 show that the dominant ions in these mass spectra are at m/z 41, 43, and 55.

Formatted: Font color: Red

Formatted: Font color: Red

Deleted: There were day-to-day differences in the Fast Food mass spectrum, with one day (Fast Food 1) being similar to other restaurants ($R = 0.7-0.8$, $\theta < 30^\circ$), and the other day (Fast Food 2) having lower R and higher θ .

Formatted: Font color: Red

Formatted: Font color: Red

486 There is also a high correlation of most restaurants with the COA PMF factor from
487 Crippa et al., (2013) ($R > \sim 0.75$, $\theta < \sim 30^\circ$). This suggests that PMF analysis of ambient datasets
488 yields a COA factor that is similar to fresh cooking emissions from many restaurants. There is a
489 high R between our COA and the PMF HOA (hydrocarbon-like OA) factor, which is
490 representative of primary combustion-related emissions. Even though m/z 41, 43, and 55 are
491 useful COA markers to resolve cooking-related factors, there are diverse sources of m/z 41, 43,
492 and 55. In general, there is a high correlation between HOA and COA because the major HOA
493 peaks like m/z 55 and 57 are prominent in both factors (Milic et al., 2016; Sun et al., 2013; D.
494 Yao et al., 2021).

495 One key difference between HOA and COA is that the HOA mass spectrum is dominated
496 by hydrocarbon (C_xH_y), whereas the cooking OA has a mixture of hydrocarbon and oxygenated
497 ions, as shown in Figure 4. For example, m/z 43 in HOA is almost entirely due to $C_3H_7^+$ (Ng et
498 al., 2010), whereas cooking OA contains both $C_3H_7^+$ and $C_2H_3O^+$ (Fig. 4). Similarly, for m/z 55,
499 COA has contributions from both hydrocarbon ($C_4H_7^+$) and oxidized ($C_3H_3O^+$) fragments
500 (Canonaco et al., 2013; Lalchandani et al., 2021), whereas the reduced ion dominates HOA.
501 Lastly, while m/z 55 and 57 are important signals for both COA and HOA, COA typically has f_{55}
502 $> f_{57}$, whereas HOA has the reverse (W. Hu et al., 2016; D. D. Huang et al., 2021a; Mohr et al.,
503 2009; Shah et al., 2018; Y. Zhang et al., 2015; Zhu et al., 2018).

504 Figure 5 also compares our cooking emissions measurements to PMF factors for biomass
505 burning (BBOA) and secondary organic aerosol (LVOOA). The majority of restaurant sites
506 exhibited weak correlations with BBOA and LVOOA. BBOA has prominent peaks at m/z 60 and
507 73, and the largest peak in the LVOOA mass spectrum is m/z 44; none of these peaks are
508 particularly large in the cooking mass spectra from the restaurant sites sampled here.

Formatted: Font color: Red

Formatted: Font color: Red

Deleted: Correlations with BBOA and LVOOA are weaker as these factors are characterized by dominant peaks at m/z 60 and 73 for BBOA and m/z 44 and 43 for LVOOA. There is a high R between our COA and the PMF HOA factor, which is representative of primary combustion-related emissions.

Deleted: ¶

3.4 Cooking as a source of urban reduced nitrogen

Cooking OA from all of the restaurant sites had a significant contribution from AMS ions containing reduced nitrogen. The mean contribution of nitrogen-containing fragments to the total cooking OA mass was 15.8% (median = 10.7%; Table S2). The bulk of these N-containing ions (95% by mass) did not contain oxygen (Fig. S6), though oxygen could still be present on the parent molecule prior to fragmentation. These $C_xH_yN^+$ fragments include $C_2H_5N^+$ (m/z 43) and $C_3H_5N^+$ (m/z 55), shown in Figure 4. For example, in the mass spectrum presented for Bar/Restaurant 1 (Figure 3), the collective contribution of the CHN family peaks is 9.2% of the total signal mass. The nitrogen-containing fragment at m/z 41, denoted as CHN_2^+ , has a 2.1% contribution. Other significant peaks include m/z 43 ($C_2H_5N^+$) at 0.77%, m/z 79 ($C_5H_5N^+$) at 0.68%, and m/z 68 ($C_4H_6N^+$) at 0.49%. For nearly all restaurants sampled here, the most abundant CHN group ion was $C_3H_8N^+$, with $f_{C_3H_8N}$ typically > 1%.

We took several steps to verify the presence of these reduced nitrogen peaks in our mass spectra. These quality assurance checks, including examples of peak fitting, are shown in section 3 of the SI. For example, Figure S8 shows the fitting of $C_3H_8N^+$ for the Bakery samples. Figure S8 shows that the CHN family peaks are not present when the AMS chopper is closed. This indicates that these signals arise from particles, and are not instrument artifacts. One potential source of reduced-N peaks is surface ionization, where atoms are ejected from a heated surface and subsequently ionized. Figure S9 shows that our peak shapes remain Gaussian, and are therefore unlikely to be influenced by surface ionization.

Previous studies have reported the existence of nitrogen compounds or fragments from cooking experiments. These nitrogen-containing compounds can originate from the food itself or reactions with the types of gas used during cooking (Abdullahi et al., 2013). Reyes-Villegas et

Commented [AP3]: C+H+N does not equal 41. What is the ion?

Formatted: Font color: Red

Formatted: Font color: Red

Deleted: For example, the mass spectrum from Bar/Restaurant 1 in Figure 2 has 9% CHN family peaks by mass, with significant contributions at m/z 41 and 43. For nearly all restaurants sampled here, the most abundant CHN group ion was $C_3H_8N^+$, with $f_{C_3H_8N}$ typically > 1%.¶

al., 2018 measured gas- and particle-phase emissions and found 14 different nitrogen-containing compounds using chemical ionization mass spectrometry. Rogge et al., 1991 measured amides in cooking emissions, including palmitamide and stearamide. Amides were also identified from both Chinese cooking (Y. Zhao et al., 2007a) and Western-style cooking (Y. Zhao et al., 2007b) using GC-MS. Ditto et al., (2022) recently demonstrated that amides can be formed from the reaction of ammonia formed by amino acid thermal degradation with triglyceride ester linkages. In contrast to the reduced nitrogen in our samples, these nitrogen-containing compounds, including amides, have at least one oxygen in their formula.

The Bakery 1 and Bakery 2 samples had the largest contributions from reduced N. Figure 6 shows the aerosol mass spectrum from Bakery 1. The two most abundant ions in the mass spectrum are $C_3H_8N^+$ (m/z 58) and $C_5H_{12}N^+$ (m/z 86); together these two ions make up ~48% of the AMS-measured OA mass spectra. There is also a large contribution from $C_6H_{14}N^+$ at m/z 100. The large abundance of these reduced N-containing peaks contributes to the low correlation between the Bakery samples and other sites in Figure 5.

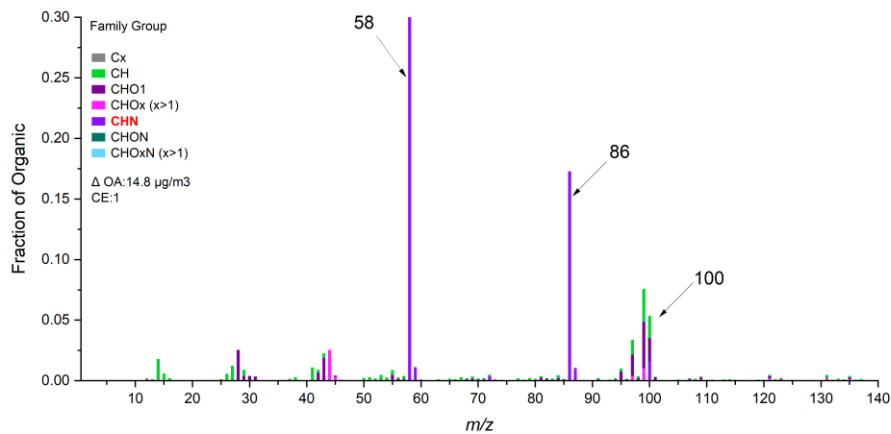


Figure 6. The aerosol mass spectrum from Bakery 1, with prominent peaks at m/z 58, 86, and 100 that are in the CHN family.

Deleted: Bakery 1

Formatted: Font color: Red

562
563 Though fast food sites have a lower correlation with other cooking sites in Figure 5, it is
564 not primarily due to higher CHN levels like bakery samples. The most abundant signals of Fast
565 Food 1 and Fast Food 2 were in the category of CHO and CH groups, where their sum accounts
566 for 73.3 % and 82.0 % of the total mass, respectively. Two samples from Fast Food sites show
567 moderate to slightly large proportions of CHN family peaks (14% and 7%) and $\text{f}_{\text{C}_3\text{H}_8\text{N}^+}$ (2.15 and
568 2.33).

569 While the $\text{C}_3\text{H}_8\text{N}^+$ fragment has been observed in all of our cooking site data, there is
570 almost no contribution of m/z 86 ($\text{C}_5\text{H}_{12}\text{N}^+$) and 100 ($\text{C}_6\text{H}_{14}\text{N}^+$) in our samples except for the two
571 bakery visits (Table S2), which were collected adjacent to a large commercial bread bakery. It is
572 thus possible that m/z 86 and 100 are more associated with commercial bakeries than restaurant
573 cooking. The underlying source of the reduced nitrogen ions, especially m/z 86 and 100 observed
574 at the bakery, is unknown. One potential source could be the use of azodicarbonamide
575 ($\text{C}_2\text{H}_4\text{N}_4\text{O}_2$, ADA), which is used as an aging and bleaching ingredient in bread baking. To test
576 whether ADA contributed to nitrogen-containing emissions from bread baking, we baked bread
577 with and without ADA addition. We used the AMS to measure the composition of PM emissions
578 during fermentation (i.e., while the bread dough rose) and baking. While we observed OA
579 emissions during baking, none of our experiments showed the CHN signals with $\text{C}_3\text{H}_8\text{N}^+$,
580 $\text{C}_5\text{H}_{12}\text{N}^+$, and $\text{C}_6\text{H}_{14}\text{N}^+$. As a result, we cannot conclude that the presence of ADA leads to high
581 proportions of CHN ions (SI Fig. 7).

582 Abundant reduced nitrogen was also observed in the particle phase via LC-TOF and LC-
583 MS/MS measurements. To supplement the online measurements of functionalized aerosol-phase
584 compounds, especially those containing nitrogen, offline analysis using LC-TOF was employed

for organic compound speciation for each restaurant site with sufficient mass loading, with soft ionization allowing for the molecular formula-level speciation of observed organic species. Based on the online AMS data showing differences in OA enhancement (Fig. 2), the samples were split into three sample groups, the six high-emitting restaurants (Bar/Res 1, Diner 2, Pizza, Bar/Res 2, Diner 1, Island Cuisine), the lower enhancement near-source cooking samples (Bakery 1, Bakery 2, Fast Food 1, Fast Food 2, Cafe), and urban samples excluding near-source cooking samples (i.e., samples taken in different neighborhoods and parks), though this likely includes cooking-related contributions to the urban background.

Figure 7a shows the ion abundance volatility distribution of the different functionalized compound classes in the 6 samples with the highest PM concentrations (Fig. 2, see Fig. S10 for other samples). Compound volatilities were estimated from the generated formulas, assuming all species were at 300 K (Y. Li et al., 2016) from each sample, and all ion abundances were normalized by the sample volume for comparison across samples. Figure 7b shows the volatility distributions of ion abundances from the three sample groups, with the six more enhanced near-source cooking samples demonstrating high ion abundance consistent with the higher mass concentrations of $PM_{2.5}$ sampled. The six enhanced cooking samples in Figure 7a show a greater abundance of I/SVOCs compared to the other two sample groups, suggestive of fresh emissions. The observed mixtures are highly functionalized, with observed species containing nitrogen, oxygen, and sulfur, but we note that the LC-TOF employed here has poor ionization efficiencies for CH and CHS compounds, which are thus not considered for this analysis of functionalized compounds.

While urban particulate matter has been shown to contain many functionalized species (Ditto et al., 2018; Ye et al., 2021), recent work has also shown cooking to be a source of

608 nitrogen and sulfur-containing species, which can be emitted in the gas-phase from foods such as
609 vegetables (Marcinkowska & Jeleń, 2022) or formed through cooking (Ditto et al., 2022; Takhar
610 et al., 2019). The urban background samples excluding cooking samples and the five lower
611 enhanced near-source cooking samples have similar volatility distributions with nitrogen-
612 containing compounds (Fig. 7b, S11), which suggests a role for cooking emissions in the
613 background functionalized OA composition in urban areas.

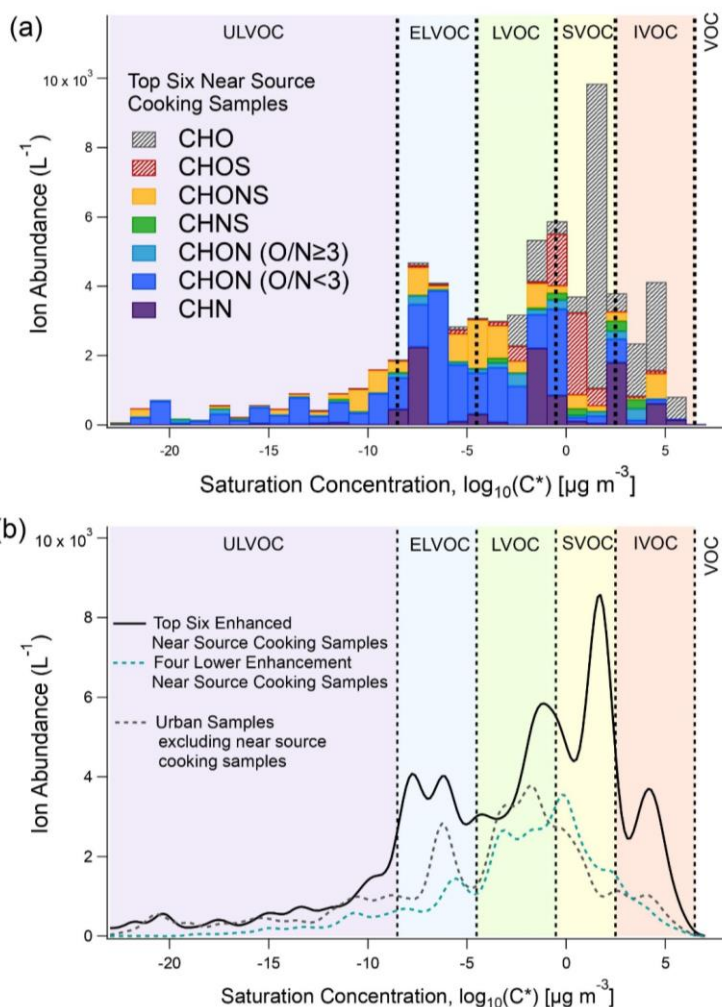


Figure 7. Averaged chemical composition of functionalized particle-phase organic compounds from (a) filters collected from the top six near-source cooking samples showing the highest enhancement in OA from the AMS measurements and (b) average ion abundance volatility distributions for the three sample groups, top six enhanced cooking samples, lower five near-source cooking samples, and the urban samples excluding near source cooking samples. Volatility bins were defined for the same reference temperature in (a) and (b) (i.e., 300 K, as all samples were collected during summertime).

623 While all samples contained nitrogen-containing compounds, LC-MS/MS was used on
624 select samples (Bakery 1, Pizza, background sample 5) from each sample group to compare the
625 functionalities of observed nitrogen. After compounds observed via LC-TOF (i.e., Fig. 7a)
626 underwent QC/QA, those compounds were selected for MS/MS analysis in a targeted mode
627 similar to prior work (Ditto et al., 2020).

628 Most nitrogen-containing compounds observed had an oxygen to nitrogen ratio (O/N) of
629 less than 3, but other nitrogen-containing compound classes were present (Fig. 7, S11). Figure 8
630 shows the observed nitrogen-containing functional groups for the three samples run on MS/MS,
631 split by O/N ratio less than 3 or greater than or equal to 3. Here, the Bakery 1 compounds
632 analyzed by MS/MS were dominated by reduced nitrogen features, with prominent amine and
633 amide functional groups, especially for compounds with O/N ratios lower than 3, which in itself
634 is indicative of the presence of reduced nitrogen structural features.

Deleted: O/N

Formatted: Font color: Red

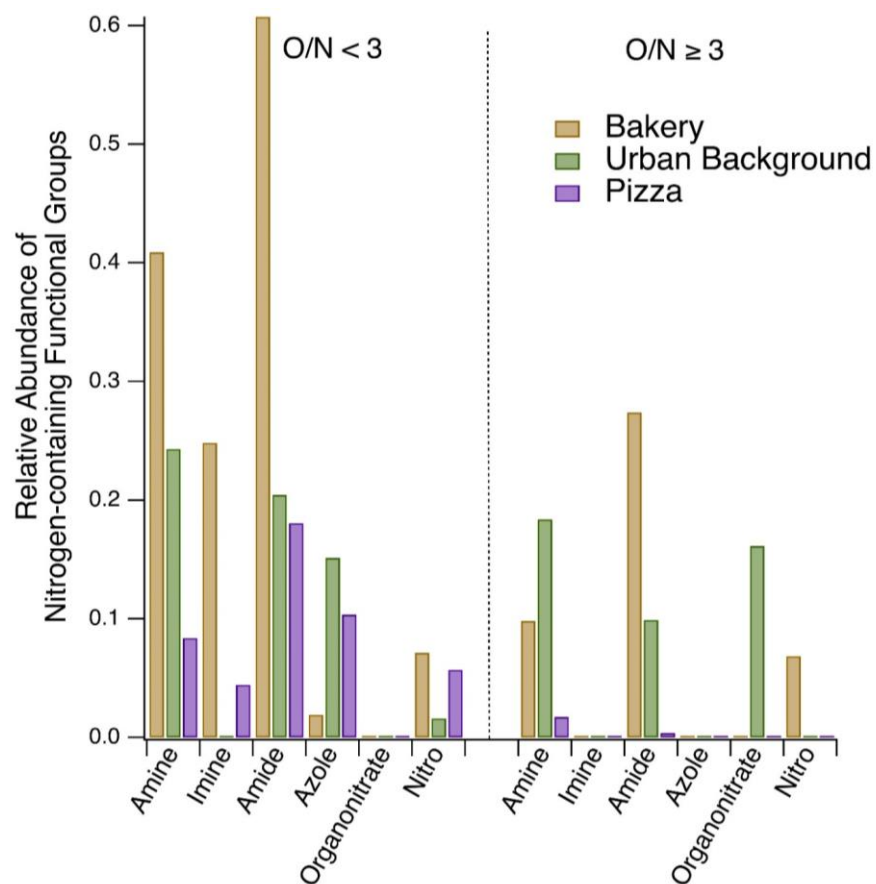


Figure 8. The relative abundance of nitrogen-containing functionalities in the Bakery 1, background sample 5, and Pizza MS/MS compounds are shown, separated by O/N ratio <3 on the left and ≥ 3 on the right, with prominently reduced nitrogen functionalities in the bakery sample. See Figure S13 for the complete range of functional groups and structural features observed in these samples. Enamine, nitrophenol, and nitrile functionalities were also searched for but were not detected in these three samples.

3.5. Particle size distributions and UFP enhancements in restaurant plumes

To expand upon Figure 1’s observations of UFPs in an example restaurant plume, we examined UFP enhancements across the sampled restaurants and the size distribution of those emissions.

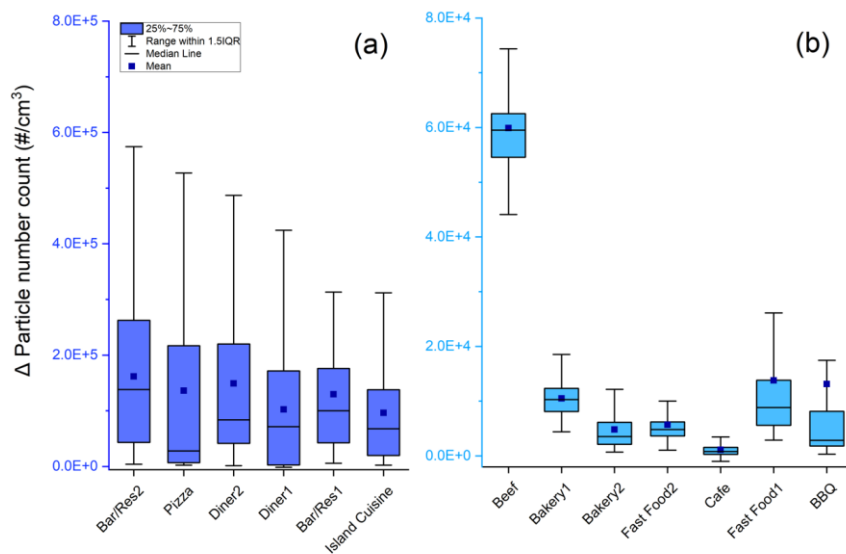


Figure 9. Particle number enhancement (Δ PNC) at each restaurant site (with IQR). The sample names in (a) and (b) are placed in the same order as in Figure 2.

Figure 9 summarizes the particle number concentrations above the background (Δ PNC) measured by the FMPS and scaled to the CPC. Similar to our Δ OA distribution in Figure 2, there are notable site-to-site differences in particle number concentrations with the sites breaking down into the higher and lower-emitting groups (high Δ PNC group mean Δ PNC $> 10^5 \#/\text{cm}^3$, low Δ PNC group mean Δ PNC $< 10^5 \#/\text{cm}^3$).

661 All of the high Δ PNC sites were also high Δ OA sites, but most sites do not have a strong
662 correlation between mean Δ OA and mean Δ PNC (Fig. S8). A moderate positive correlation was
663 observed in the time series of PNC and OA at Diner 1 ($R^2 = 0.64$), Beef (0.63), Bar/Restaurant 2
664 (0.60), and Bakery 1 (0.57); most other sites had poor correlations between Δ OA and Δ PNC (R^2
665 < 0.4). This poor correlation may indicate that the emissions of OA and PNC are decoupled
666 during cooking so that different activities boost emissions of OA mass versus particle number.
667 For example, the PNC time series in Figure 1 has several spikes that do not have associated
668 spikes in OA.

669 The PNC enhancements are less skewed than the OA enhancements. For Δ PNC, the
670 mean is always inside the IQR except for the BBQ sample, unlike several sites that had mean
671 Δ OA $> 75^{\text{th}}$ percentile. This implies that PNC emissions are less dominated by intense spikes
672 than OA emissions. Figure 2 and Figure S4 show that OA concentrations often fell close to the
673 background between spikes. PNC, on the other hand, was consistently elevated during the
674 restaurant sampling. One possible explanation is that OA spikes are associated with cooking,
675 whereas the consistently high PNC is associated with the heating of the cooking surface by either
676 a natural gas flame or electricity (Amouei Torkmahalleh et al., 2018; Dennekamp et al., 2001;
677 Wu et al., 2012).
678

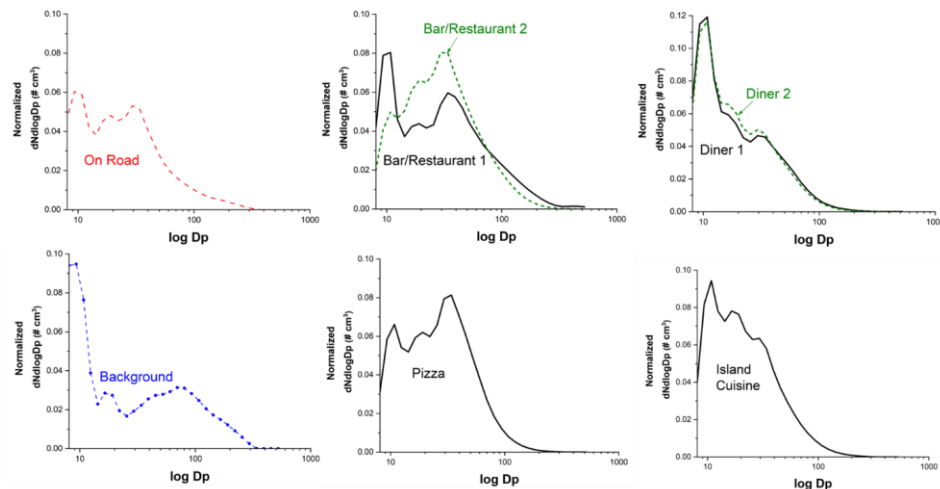


Figure 10. Mean particle size distribution comparison of on-road, background, and high Δ PNC restaurants observed at Bar/Restaurant, Diner, Pizza, and Island cuisine measured from the FMPS (Fast Mobility Particle Sizer). To fit the size distributions onto the same scale, all are normalized to the total particle number of each sampling period. Thus the integral over each of the normalized size distributions is 1.

Formatted: Font color: Red

Deleted: To fit the size distributions onto the same scale, all are normalized to the total particle number ($dN/d\log Dp$) of each sampling period over each size bin and make the sum of all normalized size distributions to be 1.

Figure 10 shows the mean particle size distributions for the “high Δ PNC” restaurants from Figure 7a and the mean on-road and background particle size distributions from the period shown in Figure 1. All the restaurants emitted UFPs. The mode particle diameter from all sampled restaurants was less than 50 nm (Table 1), and the size distributions in Figure 10 clearly peak in the ultrafine size range. However, there is variability across the restaurants as some sites had bimodal size distributions, while others are closer to unimodal. For example, Bar/Restaurant 1 has distinct modes at ~10 and 40 nm, whereas Island Cuisine has a single broad mode centered around 20 nm. There is also variability within sites. For example, Bar/Restaurant 2 has a unimodal distribution with a mode around 40 nm, and the size distribution differs from the other

sample at the same location, while the two samples at the Diner have nearly identical size distributions.

In addition to being enhanced in terms of concentrations, the size distributions in the restaurant plumes are distinct from the average background size distributions, which have a bimodal distribution with a nucleation mode peak around 10 nm and an accumulation mode peak around 100 nm. Emissions from nearby vehicles dominate the on-road periods, with a bimodal size distribution around 10 nm and 20-40 nm, which is similarly observed in previous studies (Sturm et al., 2003; Wang et al., 2008; X. Yao et al., 2005).

4. Conclusions and Atmospheric Relevance

Using mobile measurements across a range of commercial cooking operations in two cities, our real-world sampling of cooking plumes from restaurants demonstrates substantial cooking-associated aerosol emissions with variability in the concentrations, chemical composition, and size distribution of PM and UFP emissions. Overall, emissions from most restaurants had similar mass spectra both to each other and to COA factors determined from factor analysis of ambient datasets. Aerosol mass spectra of cooking emissions were generally dominated by a mix of reduced ($C_xH_y^+$) and oxygenated ($C_xH_yO^+$) ions.

There were significant site-to-site differences in the OA enhancement attributable to restaurant emissions. This variability is due to a combination of differences in the emission rate from each restaurant and in dilution between the restaurant exhaust and our sampling inlet, though we cannot quantify the importance of each process. Since at all locations our inlet was only a few meters from the restaurant exhaust, it is likely that differences in the emission rate dominate site-to-site variability. Previous research by Louvaris et al., 2017 investigated meat

charbroiling emissions diluted within a chamber and reported that approximately 80% of the COA persisted following isothermal dilution at ambient temperature (25 °C) by a factor of 10. This is consistent with much of the cooking OA being in the LVOC or ELVOC volatility range.

Reduced nitrogen (N) was prevalent across all restaurant samples, contributing approximately 15% of the cooking organic aerosol (OA) mass at the sampled sites, with a diversity of reduced N functional groups observed. The presence of these reduced nitrogen species is confirmed with offline analysis of filter samples, which identified multiple N-containing species with O/N < 3, indicating that these nitrogen containing species were unlikely to be organic nitrates. A notable finding of this study was the distinct composition of emissions collected from a commercial bakery, marked by the elevated presence of reduced nitrogen. Numerous studies have investigated cooking aerosol compositions, demonstrating that different cooking techniques and ingredients can elevate nitrogen content levels in cooking PM. (Ditto et al., 2022; Masoud et al., 2022; Reyes-Villegas et al., 2018b; Rogge et al., 1991b). Nitrogen found in cooking emissions has diverse origins, including from the food itself with both natural (e.g., protein-rich and plant-based products) (Bak et al., 2019; Han et al., 2020) and anthropogenic sources (e.g., fertilizers and food additives like nitrates and nitrites) (Dimkpa et al., 2020; Karwowska & Kononiuk, 2020). Nitrogen in cooking PM can also be formed from heterogenous reactions with thermal degradation products formed during cooking (Ditto et al., 2022).

To further examine potential sources of the nitrogen features identified from the bakery emissions, we conducted an experiment with the AMS measuring bread baking emissions both with and without the dough stabilizer azodicarbonamide (C₂H₄N₄O₂) as a potential source of N-containing peaks. While the reduced nitrogen peaks were not observed, this result implies the

Formatted: Font color: Red

Deleted: However, a notable finding of this study was the distinct composition of emissions collected from a commercial bakery, marked by the elevated presence of reduced nitrogen. Numerous studies have investigated cooking aerosol compositions, demonstrating that different cooking techniques and ingredients can elevate nitrogen content levels

Commented [AP4]: cite Ditto 2022

Formatted: Font color: Red

Deleted: , as well as from nitrogen dioxide (NO₂) and other nitrogen oxides (NO_x) emitted from gas cooking burners (H. Zhao et al., 2021), which are primarily influenced by the duration of gas cooking and the ambient air quality (Mosqueron et al., 2002).

757 challenge in determining specific sources of nitrogen-containing species, particularly in real-
758 world cooking environments, emphasizing the need for further investigation.

759 This study also highlights that cooking emissions are substantial contributors to urban
760 UFPs. Variability between sites was observed, with some sites displaying unimodal and others
761 displaying bimodal size distributions. However, there are uncertainties in identifying the
762 characteristics of UFPs from cooking emissions, such as their origin from cooking processes or
763 natural gas usage, and potential changes in particle size distributions during dilution due to the
764 evaporation of semi-volatile components. Uncontrolled dilution in this study may have
765 contributed to differences in UFP concentration and size distribution (Lipsky & Robinson, 2006).

766 In order to gain a deeper understanding of the factors influencing UFP size distribution
767 from real-world cooking sources, further investigation is warranted, taking into account aspects
768 such as restaurant proximity, food type, and order frequency. Consequently, subsequent research
769 can identify the prevalent molecular features of reduced nitrogen in cooking emissions by setting
770 constraints on specific parameters, providing a more comprehensive analysis.

771 Overall, this study underscores the importance of comprehensively understanding
772 cooking emissions, including their contribution to the PM_{2.5} mass, composition, and exposure
773 variability across urban areas, in order to develop effective strategies for mitigating their impact
774 on air quality and human health. Specifically, further research is needed to better understand the
775 role of reduced nitrogen in atmospheric emissions from cooking activities.

776
777

778 *Data availability.* All data presented in this work can be obtained by directly contacting the
779 corresponding author at apresto@andrew.cmu.edu upon request.

Formatted: Font color: Red

Deleted: While it is acknowledged that a proportion of cooking emissions may undergo evaporation during the dilution process, it is improbable that these particles will evaporate entirely. Previous research conducted by Louvaris et al (Louvaris et al., 2017) investigated meat charbroiling emissions diluted within a chamber and reported that approximately 80% of the COA persisted following isothermal dilution at ambient temperature (25 °C) by a factor of 10. In order to gain a deeper understanding of the factors influencing UFP size distribution from real-world cooking sources, further investigation is warranted, taking into account aspects such as restaurant proximity, food type, and order frequency. Consequently, subsequent research can identify the prevalent molecular features of reduced nitrogen in cooking emissions by setting constraints on specific parameters, providing a more comprehensive analysis.¶

796

797 *Author contributions.* The experimental design was done by AAP and DRG. Data collection was
798 carried out by AAP and JEM. SK performed the data analysis and compiled the instrumental
799 data. SK and AAP wrote the paper, with all authors contributing significantly to the
800 interpretation of the results, discussions, and finalization of the paper.

801

802 *Competing interests.* At least one of the (co-)authors is a member of the editorial board of
803 Atmospheric Chemistry and Physics. The peer-review process was guided by an independent
804 editor, and the authors also have no other competing interests to declare.

805

806

807 *Acknowledgments.* This research was conducted as part of the Center for Air, Climate, and
808 Energy Solutions (CACES), which was supported by the Environmental Protection Agency
809 (assistance agreement number RD83587301) to Carnegie Mellon University. We
810 acknowledge support from assistance agreement no. RD835871 awarded by the U.S.
811 Environmental Protection Agency to Yale University. This study has not been formally reviewed
812 by the EPA. The views expressed in this document are solely those of the authors and do not
813 necessarily reflect those of the agency. The EPA does not endorse any products or commercial
814 services mentioned in this publication. DRG and JEM acknowledge financial support from the
815 U.S. NSF (CBET-2011362). SK and AAP acknowledge funding support from the U.S. NSF
816 (CBET 1907446)

817

818

819

References

- Abdullahi, K. L., Delgado-Saborit, J. M., & Harrison, R. M. (2013). Emissions and indoor concentrations of particulate matter and its specific chemical components from cooking: A review. *Atmospheric Environment*, 71, 260–294. <https://doi.org/10.1016/j.atmosenv.2013.01.061>
- Actkinson, B., Ensor, K., & Griffin, R. J. (2021). SIBaR: A new method for background quantification and removal from mobile air pollution measurements. *Atmospheric Measurement Techniques*, 14(8), 5809–5821. <https://doi.org/10.5194/amt-14-5809-2021>
- Äijälä, M., Heikkinen, L., Fröhlich, R., Canonaco, F., Prévôt, A. S. H., Junninen, H., Petäjä, T., Kulmala, M., Worsnop, D., & Ehn, M. (2017). Resolving anthropogenic aerosol pollution types – deconvolution and exploratory classification of pollution events. *Atmospheric Chemistry and Physics*, 17(4), 3165–3197. <https://doi.org/10.5194/acp-17-3165-2017>
- Ali, M. U., Lin, S., Yousaf, B., Abbas, Q., Munir, M. A. M., Rashid, A., Zheng, C., Kuang, X., & Wong, M. H. (2022). Pollution characteristics, mechanism of toxicity and health effects of the ultrafine particles in the indoor environment: Current status and future perspectives. *Critical Reviews in Environmental Science and Technology*, 52(3), 436–473. <https://doi.org/10.1080/10643389.2020.1831359>
- Allan, J. D., Williams, P. I., Morgan, W. T., Martin, C. L., Flynn, M. J., Lee, J., Nemitz, E., Phillips, G. J., Gallagher, M. W., & Coe, H. (2010). Contributions from transport, solid fuel burning and cooking to primary organic aerosols in two UK cities. *Atmospheric Chemistry and Physics*, 10(2), 647–668. <https://doi.org/10.5194/acp-10-647-2010>

Amouei Torkmahalleh, M., Ospanova, S., Baibatyrova, A., Nurbay, S., Zhanakhmet, G., & Shah, D. (2018). Contributions of burner, pan, meat and salt to PM emission during grilling. *Environmental Research*, 164, 11–17. <https://doi.org/10.1016/j.envres.2018.01.044>

Apte, J. S., Messier, K. P., Gani, S., Brauer, M., Kirchstetter, T. W., Lunden, M. M., Marshall, J. D., Portier, C. J., Vermeulen, R. C. H., & Hamburg, S. P. (2017). High-Resolution Air Pollution Mapping with Google Street View Cars: Exploiting Big Data. *Environmental Science & Technology*, 51(12), 6999–7008. <https://doi.org/10.1021/acs.est.7b00891>

Bak, U. G., Nielsen, C. W., Marinho, G. S., Gregersen, Ó., Jónsdóttir, R., & Holdt, S. L. (2019). The seasonal variation in nitrogen, amino acid, protein and nitrogen-to-protein conversion factors of commercially cultivated Faroese *Saccharina latissima*. *Algal Research*, 42, 101576. <https://doi.org/10.1016/j.algal.2019.101576>

Bozzetti, C., El Haddad, I., Salameh, D., Daellenbach, K. R., Fermo, P., Gonzalez, R., Minguillón, M. C., Iinuma, Y., Poulain, L., Elser, M., Müller, E., Slowik, J. G., Jaffrezo, J.-L., Baltensperger, U., Marchand, N., & Prévôt, A. S. H. (2017). Organic aerosol source apportionment by offline-AMS over a full year in Marseille. *Atmospheric Chemistry and Physics*, 17(13), 8247–8268. <https://doi.org/10.5194/acp-17-8247-2017>

Canonaco, F., Crippa, M., Slowik, J. G., Baltensperger, U., & Prévôt, A. S. H. (2013). SoFi, an IGOR-based interface for the efficient use of the generalized multilinear engine (ME-2) for the source apportionment: ME-2 application to aerosol mass spectrometer data. *Atmospheric Measurement Techniques*, 6(12), 3649–3661. <https://doi.org/10.5194/amt-6-3649-2013>

Castillo, M. D., Kinney, P. L., Southerland, V., Arno, C. A., Crawford, K., van Donkelaar, A., Hammer, M., Martin, R. V., & Anenberg, S. C. (2021). Estimating Intra-Urban Inequities

in PM2.5-Attributable Health Impacts: A Case Study for Washington, DC. *GeoHealth*, 5(11), e2021GH000431. <https://doi.org/10.1029/2021GH000431>

Cheng, B., Wang-Li, L., Meskhidze, N., Classen, J., & Bloomfield, P. (2019). Spatial and temporal variations of PM2.5 mass closure and inorganic PM2.5 in the Southeastern U.S. *Environmental Science and Pollution Research*, 26(32), 33181–33191. <https://doi.org/10.1007/s11356-019-06437-8>

Chow, J. C., Chen, L.-W. A., Watson, J. G., Lowenthal, D. H., Magliano, K. A., Turkiewicz, K., & Lehrman, D. E. (2006). PM2.5 chemical composition and spatiotemporal variability during the California Regional PM10/PM2.5 Air Quality Study (CRPAQS). *Journal of Geophysical Research: Atmospheres*, 111(D10). <https://doi.org/10.1029/2005JD006457>

Crippa, M., DeCarlo, P. F., Slowik, J. G., Mohr, C., Heringa, M. F., Chirico, R., Poulain, L., Freutel, F., Sciare, J., Cozic, J., Di Marco, C. F., Elsasser, M., Nicolas, J. B., Marchand, N., Abidi, E., Wiedensohler, A., Drewnick, F., Schneider, J., Borrmann, S., ... Baltensperger, U. (2013). Wintertime aerosol chemical composition and source apportionment of the organic fraction in the metropolitan area of Paris. *Atmospheric Chemistry and Physics*, 13(2), 961–981. <https://doi.org/10.5194/acp-13-961-2013>

Crippa, M., El Haddad, I., Slowik, J. G., DeCarlo, P. F., Mohr, C., Heringa, M. F., Chirico, R., Marchand, N., Sciare, J., Baltensperger, U., & Prévôt, A. S. H. (2013). Identification of marine and continental aerosol sources in Paris using high resolution aerosol mass spectrometry. *Journal of Geophysical Research: Atmospheres*, 118(4), 1950–1963. <https://doi.org/10.1002/jgrd.50151>

Dallmann, T. R., Kirchstetter, T. W., DeMartini, S. J., & Harley, R. A. (2013). Quantifying On-Road Emissions from Gasoline-Powered Motor Vehicles: Accounting for the Presence of

Medium- and Heavy-Duty Diesel Trucks. *Environmental Science & Technology*, 47(23), 13873–13881. <https://doi.org/10.1021/es402875u>

Dall'Osto, M., Paglione, M., Decesari, S., Facchini, M. C., O'Dowd, C., Plass-Duellmer, C., & Harrison, R. M. (2015). On the Origin of AMS “Cooking Organic Aerosol” at a Rural Site. *Environmental Science & Technology*, 49(24), 13964–13972. <https://doi.org/10.1021/acs.est.5b02922>

Dennekamp, M., Howarth, S., Dick, C. a. J., Cherrie, J. W., Donaldson, K., & Seaton, A. (2001). Ultrafine particles and nitrogen oxides generated by gas and electric cooking. *Occupational and Environmental Medicine*, 58(8), 511–516. <https://doi.org/10.1136/oem.58.8.511>

Devarakonda, S., Sevusu, P., Liu, H., Liu, R., Iftode, L., & Nath, B. (2013). Real-time air quality monitoring through mobile sensing in metropolitan areas. *Proceedings of the 2nd ACM SIGKDD International Workshop on Urban Computing*, 1–8. <https://doi.org/10.1145/2505821.2505834>

Dimkpa, C. O., Fugice, J., Singh, U., & Lewis, T. D. (2020). Development of fertilizers for enhanced nitrogen use efficiency – Trends and perspectives. *Science of The Total Environment*, 731, 139113. <https://doi.org/10.1016/j.scitotenv.2020.139113>

Ditto, J. C., Abbatt, J. P. D., & Chan, A. W. H. (2022). Gas- and Particle-Phase Amide Emissions from Cooking: Mechanisms and Air Quality Impacts. *Environmental Science & Technology*, 56(12), 7741–7750. <https://doi.org/10.1021/acs.est.2c01409>

Ditto, J. C., Barnes, E. B., Khare, P., Takeuchi, M., Joo, T., Bui, A. A. T., Lee-Taylor, J., Eris, G., Chen, Y., Aumont, B., Jimenez, J. L., Ng, N. L., Griffin, R. J., & Gentner, D. R. (2018). An omnipresent diversity and variability in the chemical composition of

atmospheric functionalized organic aerosol. *Communications Chemistry*, *1*(1), Article 1.
<https://doi.org/10.1038/s42004-018-0074-3>

Ditto, J. C., Joo, T., Slade, J. H., Shepson, P. B., Ng, N. L., & Gentner, D. R. (2020).
 Nontargeted Tandem Mass Spectrometry Analysis Reveals Diversity and Variability in
 Aerosol Functional Groups across Multiple Sites, Seasons, and Times of Day.
Environmental Science & Technology Letters, *7*(2), 60–69.
<https://doi.org/10.1021/acs.estlett.9b00702>

Dührkop, K., Fleischauer, M., Ludwig, M., Aksenov, A. A., Melnik, A. V., Meusel, M.,
 Dorrestein, P. C., Rousu, J., & Böcker, S. (2019). SIRIUS 4: A rapid tool for turning
 tandem mass spectra into metabolite structure information. *Nature Methods*, *16*(4),
 Article 4. <https://doi.org/10.1038/s41592-019-0344-8>

Dührkop, K., Shen, H., Meusel, M., Rousu, J., & Böcker, S. (2015). Searching molecular
 structure databases with tandem mass spectra using CSI:FingerID. *Proceedings of the
 National Academy of Sciences*, *112*(41), 12580–12585.
<https://doi.org/10.1073/pnas.1509788112>

Florou, K., Papanastasiou, D. K., Pikridas, M., Kaltsonoudis, C., Louvaris, E., Gkatzelis, G. I.,
 Patoulas, D., Mihalopoulos, N., & Pandis, S. N. (2017). The contribution of wood
 burning and other pollution sources to wintertime organic aerosol levels in two Greek
 cities. *Atmospheric Chemistry and Physics*, *17*(4), 3145–3163.
<https://doi.org/10.5194/acp-17-3145-2017>

Font, A., Guiseppin, L., Blangiardo, M., Ghersi, V., & Fuller, G. W. (2019). A tale of two cities:
 Is air pollution improving in Paris and London? *Environmental Pollution*, *249*, 1–12.
<https://doi.org/10.1016/j.envpol.2019.01.040>

Giorio, C., Tapparo, A., Dall'Osto, M., Harrison, R. M., Beddows, D. C. S., Di Marco, C., & Nemitz, E. (2012). Comparison of three techniques for analysis of data from an Aerosol Time-of-Flight Mass Spectrometer. *Atmospheric Environment*, 61, 316–326. <https://doi.org/10.1016/j.atmosenv.2012.07.054>

Han, Y., Feng, G., Swaney, D. P., Dentener, F., Koeble, R., Ouyang, Y., & Gao, W. (2020). Global and regional estimation of net anthropogenic nitrogen inputs (NANI). *Geoderma*, 361, 114066. <https://doi.org/10.1016/j.geoderma.2019.114066>

Hayes, P. L., Ortega, A. M., Cubison, M. J., Froyd, K. D., Zhao, Y., Cliff, S. S., Hu, W. W., Toohey, D. W., Flynn, J. H., Lefer, B. L., Grossberg, N., Alvarez, S., Rappenglück, B., Taylor, J. W., Allan, J. D., Holloway, J. S., Gilman, J. B., Kuster, W. C., de Gouw, J. A., ... Jimenez, J. L. (2013). Organic aerosol composition and sources in Pasadena, California, during the 2010 CalNex campaign. *Journal of Geophysical Research: Atmospheres*, 118(16), 9233–9257. <https://doi.org/10.1002/jgrd.50530>

Hering, S. V., Lewis, G. S., Spielman, S. R., & Eiguren-Fernandez, A. (2019). A MAGIC concept for self-sustained, water-based, ultrafine particle counting. *Aerosol Science and Technology*, 53(1), 63–72. <https://doi.org/10.1080/02786826.2018.1538549>

Hu, R., Wang, S., Zheng, H., Zhao, B., Liang, C., Chang, X., Jiang, Y., Yin, R., Jiang, J., & Hao, J. (2021). Variations and Sources of Organic Aerosol in Winter Beijing under Markedly Reduced Anthropogenic Activities During COVID-2019. *Environmental Science & Technology*. <https://doi.org/10.1021/acs.est.1c05125>

Hu, W., Hu, M., Hu, W., Jimenez, J. L., Yuan, B., Chen, W., Wang, M., Wu, Y., Chen, C., Wang, Z., Peng, J., Zeng, L., & Shao, M. (2016). Chemical composition, sources, and aging process of submicron aerosols in Beijing: Contrast between summer and winter.

Journal of Geophysical Research: Atmospheres, 121(4), 1955–1977.

<https://doi.org/10.1002/2015JD024020>

Huang, D. D., Zhu, S., An, J., Wang, Q., Qiao, L., Zhou, M., He, X., Ma, Y., Sun, Y., Huang, C.,

Yu, J. Z., & Zhang, Q. (2021b). Comparative Assessment of Cooking Emission

Contributions to Urban Organic Aerosol Using Online Molecular Tracers and Aerosol

Mass Spectrometry Measurements. *Environmental Science & Technology*, 55(21),

14526–14535. <https://doi.org/10.1021/acs.est.1c03280>

Huang, X.-F., He, L.-Y., Hu, M., Canagaratna, M. R., Sun, Y., Zhang, Q., Zhu, T., Xue, L.,

Zeng, L.-W., Liu, X.-G., Zhang, Y.-H., Jayne, J. T., Ng, N. L., & Worsnop, D. R. (2010).

Highly time-resolved chemical characterization of atmospheric submicron particles

during 2008 Beijing Olympic Games using an Aerodyne High-Resolution Aerosol Mass

Spectrometer. *Atmospheric Chemistry and Physics*, 10(18), 8933–8945.

<https://doi.org/10.5194/acp-10-8933-2010>

Ibald-Mulli, A., Wichmann, H.-E., Kreyling, W., & Peters, A. (2002). Epidemiological Evidence

on Health Effects of Ultrafine Particles. *Journal of Aerosol Medicine*, 15(2), 189–201.

<https://doi.org/10.1089/089426802320282310>

Jeong, C.-H., Wang, J. M., & Evans, G. J. (2016). Source Apportionment of Urban Particulate

Matter using Hourly Resolved Trace Metals, Organics, and Inorganic Aerosol

Components. *Atmospheric Chemistry and Physics Discussions*, 1–32.

<https://doi.org/10.5194/acp-2016-189>

Jung, C.-C., & Su, H.-J. (2020). Chemical and stable isotopic characteristics of PM_{2.5} emitted

from Chinese cooking. *Environmental Pollution*, 267, 115577.

<https://doi.org/10.1016/j.envpol.2020.115577>

980 [Kaltsonoudis, C., Kostenidou, E., Louvaris, E., Psichoudaki, M., Tsiligiannis, E., Florou, K.,](#)
 981 [Liangou, A., & Pandis, S. N. \(2017\). Characterization of fresh and aged organic aerosol](#)
 982 [emissions from meat charbroiling. *Atmospheric Chemistry and Physics*, 17\(11\), 7143–](#)
 983 [7155. <https://doi.org/10.5194/acp-17-7143-2017>](#)
 984 [Karwowska, M., & Kononiuk, A. \(2020\). Nitrates/Nitrites in Food—Risk for Nitrosative Stress](#)
 985 [and Benefits. *Antioxidants*, 9\(3\), Article 3. <https://doi.org/10.3390/antiox9030241>](#)
 986 [Keuken, M. P., Roemer, M. G. M., Zandveld, P., Verbeek, R. P., & Velders, G. J. M. \(2012\).](#)
 987 [Trends in primary NO₂ and exhaust PM emissions from road traffic for the period 2000–](#)
 988 [2020 and implications for air quality and health in the Netherlands. *Atmospheric*](#)
 989 [*Environment*, 54, 313–319. <https://doi.org/10.1016/j.atmosenv.2012.02.009>](#)
 990 [Kiendler-Scharr, A., Zhang, Q., Hohaus, T., Kleist, E., Mensah, A., Mentel, T. F., Spindler, C.,](#)
 991 [Uerlings, R., Tillmann, R., & Wildt, J. \(2009\). Aerosol Mass Spectrometric Features of](#)
 992 [Biogenic SOA: Observations from a Plant Chamber and in Rural Atmospheric](#)
 993 [Environments. *Environmental Science & Technology*, 43\(21\), 8166–8172.](#)
 994 [<https://doi.org/10.1021/es901420b>](#)
 995 [Klompaker, J. O., Montagne, D. R., Meliefste, K., Hoek, G., & Brunekreef, B. \(2015\). Spatial](#)
 996 [variation of ultrafine particles and black carbon in two cities: Results from a short-term](#)
 997 [measurement campaign. *Science of The Total Environment*, 508, 266–275.](#)
 998 [<https://doi.org/10.1016/j.scitotenv.2014.11.088>](#)
 999 [Kostenidou, E., Lee, B.-H., Engelhart, G. J., Pierce, J. R., & Pandis, S. N. \(2009\). Mass Spectra](#)
 1000 [Deconvolution of Low, Medium, and High Volatility Biogenic Secondary Organic](#)
 1001 [Aerosol. *Environmental Science & Technology*, 43\(13\), 4884–4889.](#)
 1002 [<https://doi.org/10.1021/es803676g>](#)

1003 Kwon, H.-S., Ryu, M. H., & Carlsten, C. (2020). Ultrafine particles: Unique physicochemical
 1004 properties relevant to health and disease. *Experimental & Molecular Medicine*, 52(3),
 1005 Article 3. <https://doi.org/10.1038/s12276-020-0405-1>

1006 Lalchandani, V., Kumar, V., Tobler, A., M. Thamban, N., Mishra, S., Slowik, J. G., Bhattu, D.,
 1007 Rai, P., Satish, R., Ganguly, D., Tiwari, S., Rastogi, N., Tiwari, S., Močnik, G., Prévôt,
 1008 A. S. H., & Tripathi, S. N. (2021). Real-time characterization and source apportionment
 1009 of fine particulate matter in the Delhi megacity area during late winter. *Science of The*
 1010 *Total Environment*, 770, 145324. <https://doi.org/10.1016/j.scitotenv.2021.145324>

1011 Lanz, V. A., Alfarra, M. R., Baltensperger, U., Buchmann, B., Hueglin, C., & Prévôt, A. S. H.
 1012 (2007). Source apportionment of submicron organic aerosols at an urban site by factor
 1013 analytical modelling of aerosol mass spectra. *Atmospheric Chemistry and Physics*, 7(6),
 1014 1503–1522. <https://doi.org/10.5194/acp-7-1503-2007>

1015 Lee, B. P., Li, Y. J., Yu, J. Z., Louie, P. K. K., & Chan, C. K. (2015). Characteristics of
 1016 submicron particulate matter at the urban roadside in downtown Hong Kong—Overview
 1017 of 4 months of continuous high-resolution aerosol mass spectrometer measurements.
 1018 *Journal of Geophysical Research: Atmospheres*, 120(14), 7040–7058.
 1019 <https://doi.org/10.1002/2015JD023311>

1020 Lenschow, P., Abraham, H.-J., Kutzner, K., Lutz, M., Preuß, J.-D., & Reichenbacher, W. (2001).
 1021 Some ideas about the sources of PM10. *Atmospheric Environment*, 35, S23–S33.
 1022 [https://doi.org/10.1016/S1352-2310\(01\)00122-4](https://doi.org/10.1016/S1352-2310(01)00122-4)

1023 Li, Y., Pöschl, U., & Shiraiwa, M. (2016). Molecular corridors and parameterizations of
 1024 volatility in the chemical evolution of organic aerosols. *Atmospheric Chemistry and*
 1025 *Physics*, 16(5), 3327–3344. <https://doi.org/10.5194/acp-16-3327-2016>

- Li, Z., Fung, J. C. H., & Lau, A. K. H. (2018). High spatiotemporal characterization of on-road PM_{2.5} concentrations in high-density urban areas using mobile monitoring. *Building and Environment*, 143, 196–205. <https://doi.org/10.1016/j.buildenv.2018.07.014>
- Liu, T., Li, Z., Chan, M., & Chan, C. K. (2017). Formation of secondary organic aerosols from gas-phase emissions of heated cooking oils. *Atmospheric Chemistry and Physics*, 17(12), 7333–7344. <https://doi.org/10.5194/acp-17-7333-2017>
- Liu, T., Wang, Z., Wang, X., & Chan, C. K. (2018). Primary and secondary organic aerosol from heated cooking oil emissions. *Atmospheric Chemistry and Physics*, 18(15), 11363–11374. <https://doi.org/10.5194/acp-18-11363-2018>
- Louie, P. K. K., Chow, J. C., Chen, L.-W. A., Watson, J. G., Leung, G., & Sin, D. W. M. (2005). PM_{2.5} chemical composition in Hong Kong: Urban and regional variations. *Science of The Total Environment*, 338(3), 267–281. <https://doi.org/10.1016/j.scitotenv.2004.07.021>
- Louvaris, E. E., Karnezi, E., Kostenidou, E., Kaltsonoudis, C., & Pandis, S. N. (2017). Estimation of the volatility distribution of organic aerosol combining thermodenuder and isothermal dilution measurements. *Atmospheric Measurement Techniques*, 10(10), 3909–3918. <https://doi.org/10.5194/amt-10-3909-2017>
- Marcinkowska, M. A., & Jeleń, H. H. (2022). Role of Sulfur Compounds in Vegetable and Mushroom Aroma. *Molecules*, 27(18), Article 18. <https://doi.org/10.3390/molecules27186116>
- Masoud, C. G., Li, Y., Wang, D. S., Katz, E. F., DeCarlo, P. F., Farmer, D. K., Vance, M. E., Shiraiwa, M., & Hildebrandt Ruiz, L. (2022). Molecular composition and gas-particle partitioning of indoor cooking aerosol: Insights from a FIGAERO-CIMS and kinetic

aerosol modeling. *Aerosol Science and Technology*, 0(0), 1–18.

<https://doi.org/10.1080/02786826.2022.2133593>

Milic, A., Miljevic, B., Alroe, J., Mallet, M., Canonaco, F., Prevot, A. S. H., & Ristovski, Z. D.

(2016). The ambient aerosol characterization during the prescribed bushfire season in

Brisbane 2013. *Science of The Total Environment*, 560–561, 225–232.

<https://doi.org/10.1016/j.scitotenv.2016.04.036>

Mohr, C., Huffman, J. A., Cubison, M. J., Aiken, A. C., Docherty, K. S., Kimmel, J. R., Ulbrich,

I. M., Hannigan, M., & Jimenez, J. L. (2009). Characterization of Primary Organic

Aerosol Emissions from Meat Cooking, Trash Burning, and Motor Vehicles with High-

Resolution Aerosol Mass Spectrometry and Comparison with Ambient and Chamber

Observations. *Environmental Science & Technology*, 43(7), 2443–2449.

<https://doi.org/10.1021/es8011518>

Mohr, C., Richter, R., DeCarlo, P. F., Prévôt, A. S. H., & Baltensperger, U. (2011). Spatial

variation of chemical composition and sources of submicron aerosol in Zurich during

wintertime using mobile aerosol mass spectrometer data. *Atmospheric Chemistry and*

Physics, 11(15), 7465–7482. <https://doi.org/10.5194/acp-11-7465-2011>

N. Pandis, S., Skyllakou, K., Florou, K., Kostenidou, E., Kaltsonoudis, C., Hasa, E., & A. Presto,

A. (2016). Urban particulate matter pollution: A tale of five cities. *Faraday Discussions*,

189(0), 277–290. <https://doi.org/10.1039/C5FD00212E>

Omelekhina, Y., Eriksson, A., Canonaco, F., H. Prevot, A. S., Nilsson, P., Isaxon, C., Pagels, J.,

& Wierzbicka, A. (2020). Cooking and electronic cigarettes leading to large differences

between indoor and outdoor particle composition and concentration measured by aerosol

mass spectrometry. *Environmental Science: Processes & Impacts*, 22(6), 1382–1396.

<https://doi.org/10.1039/D0EM00061B>

Raatikainen, T., Vaattovaara, P., Tiitta, P., Miettinen, P., Rautiainen, J., Ehn, M., Kulmala, M.,

Laaksonen, A., & Worsnop, D. R. (2010). Physicochemical properties and origin of

organic groups detected in boreal forest using an aerosol mass spectrometer. *Atmospheric*

Chemistry and Physics, 10(4), 2063–2077. <https://doi.org/10.5194/acp-10-2063-2010>

Renzi, M., Marchetti, S., de' Donato, F., Pappagallo, M., Scortichini, M., Davoli, M., Frova, L.,

Michelozzi, P., & Stafoggia, M. (2021). Acute Effects of Particulate Matter on All-Cause

Mortality in Urban, Rural, and Suburban Areas, Italy. *International Journal of*

Environmental Research and Public Health, 18(24), Article 24.

<https://doi.org/10.3390/ijerph182412895>

Reyes-Villegas, E., Bannan, T., Le Breton, M., Mehra, A., Priestley, M., Percival, C., Coe, H., &

Allan, J. D. (2018a). Online Chemical Characterization of Food-Cooking Organic

Aerosols: Implications for Source Apportionment. *Environmental Science & Technology*,

52(9), 5308–5318. <https://doi.org/10.1021/acs.est.7b06278>

Reyes-Villegas, E., Bannan, T., Le Breton, M., Mehra, A., Priestley, M., Percival, C., Coe, H., &

Allan, J. D. (2018b). Online Chemical Characterization of Food-Cooking Organic

Aerosols: Implications for Source Apportionment. *Environmental Science & Technology*,

52(9), 5308–5318. <https://doi.org/10.1021/acs.est.7b06278>

Rogge, W. F., Hildemann, L. M., Mazurek, M. A., Cass, G. R., & Simoneit, B. R. T. (1991a).

Sources of fine organic aerosol. 1. Charbroilers and meat cooking operations.

Environmental Science & Technology, 25(6), 1112–1125.

<https://doi.org/10.1021/es00018a015>

Rogge, W. F., Hildemann, L. M., Mazurek, M. A., Cass, G. R., & Simoneit, B. R. T. (1991b).
 Sources of fine organic aerosol. 1. Charbroilers and meat cooking operations.
Environmental Science & Technology, 25(6), 1112–1125.
<https://doi.org/10.1021/es00018a015>

Rose Eilenberg, S., Subramanian, R., Malings, C., Haurlyuk, A., Presto, A. A., & Robinson, A.
 L. (2020). Using a network of lower-cost monitors to identify the influence of modifiable
 factors driving spatial patterns in fine particulate matter concentrations in an urban
 environment. *Journal of Exposure Science & Environmental Epidemiology*, 30(6), Article
 6. <https://doi.org/10.1038/s41370-020-0255-x>

Ruggeri, G., & Takahama, S. (2016). Technical Note: Development of chemoinformatic tools to
 enumerate functional groups in molecules for organic aerosol characterization.
Atmospheric Chemistry and Physics, 16(7), 4401–4422. <https://doi.org/10.5194/acp-16-4401-2016>

Saha, P. K., Sengupta, S., Adams, P., Robinson, A. L., & Presto, A. A. (2020). Spatial
 Correlation of Ultrafine Particle Number and Fine Particle Mass at Urban Scales:
 Implications for Health Assessment. *Environmental Science & Technology*, 54(15),
 9295–9304. <https://doi.org/10.1021/acs.est.0c02763>

Saha, P. K., Zimmerman, N., Malings, C., Haurlyuk, A., Li, Z., Snell, L., Subramanian, R.,
 Lipsky, E., Apte, J. S., Robinson, A. L., & Presto, A. A. (2019). Quantifying high-
 resolution spatial variations and local source impacts of urban ultrafine particle
 concentrations. *Science of The Total Environment*, 655, 473–481.
<https://doi.org/10.1016/j.scitotenv.2018.11.197>

Schauer, J. J., Kleeman, M. J., Cass, G. R., & Simoneit, B. R. T. (2002). Measurement of Emissions from Air Pollution Sources. 4. C1–C27 Organic Compounds from Cooking with Seed Oils. *Environmental Science & Technology*, 36(4), 567–575. <https://doi.org/10.1021/es002053m>

Schauer, J. J., Rogge, W. F., Hildemann, L. M., Mazurek, M. A., Cass, G. R., & Simoneit, B. R. T. (1996). Source apportionment of airborne particulate matter using organic compounds as tracers. *Atmospheric Environment*, 30(22), 3837–3855. [https://doi.org/10.1016/1352-2310\(96\)00085-4](https://doi.org/10.1016/1352-2310(96)00085-4)

Schraufnagel, D. E. (2020). The health effects of ultrafine particles. *Experimental & Molecular Medicine*, 52(3), Article 3. <https://doi.org/10.1038/s12276-020-0403-3>

Shah, R. U., Robinson, E. S., Gu, P., Robinson, A. L., Apte, J. S., & Presto, A. A. (2018). High-spatial-resolution mapping and source apportionment of aerosol composition in Oakland, California, using mobile aerosol mass spectrometry. *Atmospheric Chemistry and Physics*, 18(22), 16325–16344. <https://doi.org/10.5194/acp-18-16325-2018>

Song, R., Presto, A. A., Saha, P., Zimmerman, N., Ellis, A., & Subramanian, R. (2021a). Spatial variations in urban air pollution: Impacts of diesel bus traffic and restaurant cooking at small scales. *Air Quality, Atmosphere & Health*, 14(12), 2059–2072. <https://doi.org/10.1007/s11869-021-01078-8>

Song, R., Presto, A. A., Saha, P., Zimmerman, N., Ellis, A., & Subramanian, R. (2021b). Spatial variations in urban air pollution: Impacts of diesel bus traffic and restaurant cooking at small scales. *Air Quality, Atmosphere & Health*. <https://doi.org/10.1007/s11869-021-01078-8>

Sturm, P. J., Baltensperger, U., Bacher, M., Lechner, B., Hausberger, S., Heiden, B., Imhof, D.,
 Weingartner, E., Prevot, A. S. H., Kurtenbach, R., & Wiesen, P. (2003). Roadside
 measurements of particulate matter size distribution. *Atmospheric Environment*, 37(37),
 5273–5281. <https://doi.org/10.1016/j.atmosenv.2003.05.006>
 Sun, Y. L., Wang, Z. F., Fu, P. Q., Yang, T., Jiang, Q., Dong, H. B., Li, J., & Jia, J. J. (2013).
 Aerosol composition, sources and processes during wintertime in Beijing, China.
Atmospheric Chemistry and Physics, 13(9), 4577–4592. [https://doi.org/10.5194/acp-13-](https://doi.org/10.5194/acp-13-4577-2013)
 4577-2013
 Sun, Y. L., Zhang, Q., Schwab, J. J., Yang, T., Ng, N. L., & Demerjian, K. L. (2012). Factor
 analysis of combined organic and inorganic aerosol mass spectra from high resolution
 aerosol mass spectrometer measurements. *Atmospheric Chemistry and Physics*, 12(18),
 8537–8551. <https://doi.org/10.5194/acp-12-8537-2012>
 Takhar, M., Stroud, C. A., & Chan, A. W. H. (2019). Volatility Distribution and Evaporation
 Rates of Organic Aerosol from Cooking Oils and their Evolution upon Heterogeneous
 Oxidation. *ACS Earth and Space Chemistry*, 3(9), 1717–1728.
<https://doi.org/10.1021/acsearthspacechem.9b00110>
 Tan, Y., Dallmann, T. R., Robinson, A. L., & Presto, A. A. (2016). Application of plume
 analysis to build land use regression models from mobile sampling to improve model
 transferability. *Atmospheric Environment*, 134, 51–60.
<https://doi.org/10.1016/j.atmosenv.2016.03.032>
 Torkmahalleh, M. A., Goldasteh, I., Zhao, Y., Udochu, N. M., Rossner, A., Hopke, P. K., &
 Ferro, A. R. (2012). PM_{2.5} and ultrafine particles emitted during heating of commercial

1159 [cooking oils. *Indoor Air*, 22\(6\), 483–491. https://doi.org/10.1111/j.1600-](#)
1160 [0668.2012.00783.x](#)

1161 [Wallace, L. A., Emmerich, S. J., & Howard-Reed, C. \(2004\). Source Strengths of Ultrafine and](#)
1162 [Fine Particles Due to Cooking with a Gas Stove. *Environmental Science & Technology*,](#)
1163 [38\(8\), 2304–2311. https://doi.org/10.1021/es0306260](#)

1164 [Wan, M.-P., Wu, C.-L., Sze To, G.-N., Chan, T.-C., & Chao, C. Y. H. \(2011\). Ultrafine particles,](#)
1165 [and PM2.5 generated from cooking in homes. *Atmospheric Environment*, 45\(34\), 6141–](#)
1166 [6148. https://doi.org/10.1016/j.atmosenv.2011.08.036](#)

1167 [Wang, Y., Bechle, M. J., Kim, S.-Y., Adams, P. J., Pandis, S. N., Pope, C. A., Robinson, A. L.,](#)
1168 [Sheppard, L., Szpiro, A. A., & Marshall, J. D. \(2020\). Spatial decomposition analysis of](#)
1169 [NO2 and PM2.5 air pollution in the United States. *Atmospheric Environment*, 241,](#)
1170 [117470. https://doi.org/10.1016/j.atmosenv.2020.117470](#)

1171 [Wang, Y., Zhu, Y., Salinas, R., Ramirez, D., Karnae, S., & John, K. \(2008\). Roadside](#)
1172 [Measurements of Ultrafine Particles at a Busy Urban Intersection. *Journal of the Air &*](#)
1173 [Waste Management Association, 58\(11\), 1449–1457. https://doi.org/10.3155/1047-](#)
1174 [3289.58.11.1449](#)

1175 [Wu, C. L., Chao, C. Y. H., Sze-To, G. N., Wan, M. P., & Chan, T. C. \(2012\). Ultrafine Particle](#)
1176 [Emissions from Cigarette Smouldering, Incense Burning, Vacuum Cleaner Motor](#)
1177 [Operation and Cooking. *Indoor and Built Environment*, 21\(6\), 782–796.](#)
1178 [https://doi.org/10.1177/1420326X11421356](#)

1179 [Yao, D., Lyu, X., Lu, H., Zeng, L., Liu, T., Chan, C. K., & Guo, H. \(2021\). Characteristics,](#)
1180 [sources and evolution processes of atmospheric organic aerosols at a roadside site in](#)

Hong Kong. *Atmospheric Environment*, 252, 118298.

<https://doi.org/10.1016/j.atmosenv.2021.118298>

Yao, X., Lau, N. T., Fang, M., & Chan, C. K. (2005). Real-Time Observation of the Transformation of Ultrafine Atmospheric Particle Modes. *Aerosol Science and Technology*, 39(9), 831–841. <https://doi.org/10.1080/02786820500295248>

Ye, C., Yuan, B., Lin, Y., Wang, Z., Hu, W., Li, T., Chen, W., Wu, C., Wang, C., Huang, S., Qi, J., Wang, B., Wang, C., Song, W., Wang, X., Zheng, E., Krechmer, J. E., Ye, P., Zhang, Z., ... Shao, M. (2021). Chemical characterization of oxygenated organic compounds in the gas phase and particle phase using iodide CIMS with FIGAERO in urban air. *Atmospheric Chemistry and Physics*, 21(11), 8455–8478. <https://doi.org/10.5194/acp-21-8455-2021>

Zhang, Y., Tang, L., Yu, H., Wang, Z., Sun, Y., Qin, W., Chen, W., Chen, C., Ding, A., Wu, J., Ge, S., Chen, C., & Zhou, H. (2015). Chemical composition, sources and evolution processes of aerosol at an urban site in Yangtze River Delta, China during wintertime. *Atmospheric Environment*, 123, 339–349. <https://doi.org/10.1016/j.atmosenv.2015.08.017>

Zhang, Z., Zhu, W., Hu, M., Wang, H., Chen, Z., Shen, R., Yu, Y., Tan, R., & Guo, S. (2021). Secondary Organic Aerosol from Typical Chinese Domestic Cooking Emissions. *Environmental Science & Technology Letters*, 8(1), 24–31. <https://doi.org/10.1021/acs.estlett.0c00754>

Zhao, Y., Hu, M., Slanina, S., & Zhang, Y. (2007a). Chemical Compositions of Fine Particulate Organic Matter Emitted from Chinese Cooking. *Environmental Science & Technology*, 41(1), 99–105. <https://doi.org/10.1021/es0614518>

1204 Zhao, Y., Hu, M., Slanina, S., & Zhang, Y. (2007b). The molecular distribution of fine
 1205 particulate organic matter emitted from Western-style fast food cooking. *Atmospheric*
 1206 *Environment*, 41(37), 8163–8171. <https://doi.org/10.1016/j.atmosenv.2007.06.029>
 1207 Zhu, Q., Huang, X.-F., Cao, L.-M., Wei, L.-T., Zhang, B., He, L.-Y., Elser, M., Canonaco, F.,
 1208 Slowik, J. G., Bozzetti, C., El-Haddad, I., & Prévôt, A. S. H. (2018). Improved source
 1209 apportionment of organic aerosols in complex urban air pollution using the multilinear
 1210 engine (ME-2). *Atmospheric Measurement Techniques*, 11(2), 1049–1060.
 1211 <https://doi.org/10.5194/amt-11-1049-2018>

Deleted: Abdullahi, K. L., Delgado-Saborit, J. M., & Harrison, R. M. (2013). Emissions and indoor concentrations of particulate matter and its specific chemical components from cooking: A review. *Atmospheric Environment*, 71, 260–294. <https://doi.org/10.1016/j.atmosenv.2013.01.061>¶
 Äijälä, M., Heikkinen, L., Fröhlich, R., Canonaco, F., Prévôt, A. S. H., Junninen, H., Petäjä, T., Kulmala, M., Worsnop, D., & Ehn, M. (2017). Resolving anthropogenic aerosol pollution types – deconvolution and exploratory classification of pollution events. *Atmospheric Chemistry and Physics*, 17(4), 3165–3197. <https://doi.org/10.5194/acp-17-3165-2017>¶
 Ali, M. U., Lin, S., Yousaf, B., Abbas, Q., Munir, M. A. M., Rashid, A., Zheng, C., Kuang, X., & Wong, M. H. (2022). Pollution characteristics, mechanism of toxicity and health effects of the ultrafine particles in the indoor environment: Current status and future perspectives. *Critical Reviews in Environmental Science and Technology*, 52(3), 436–473. <https://doi.org/10.1080/10643389.2020.1831359>¶
 Allan, J. D., Williams, P. I., Morgan, W. T., Martin, C. L., Flynn, M. J., Lee, J., Nemitz, E., Phillips, G. J., Gallagher, M. W., & Coe, H. (2010). Contributions from transport, solid fuel burning and cooking to primary organic aerosols in two UK cities. *Atmospheric Chemistry and Physics*, 10(2), 647–668. <https://doi.org/10.5194/acp-10-647-2010>¶
 Amouei Torkmahalleh, M., Ospanova, S., Baibatyrova, A., Nurbay, S., Zhanakhmet, G., & Shah, D. (2018). Contributions of burner, pan, meat and salt to PM emission during grilling. *Environmental Research*, 164, 11–17. <https://doi.org/10.1016/j.envres.2018.01.044>¶
 Apte, J. S., Messier, K. P., Gani, S., Brauer, M., Kirchstetter, T. W., Lunden, M. M., Marshall, J. D., Portier, C. J., Vermeulen, R. C. H., & Hamburg, S. P. (2017). High-Resolution Air Pollution Mapping with Google Street View Cars: Exploiting Big Data. *Environmental Science & Technology*, 51(12), 6999–7008. <https://doi.org/10.1021/acs.est.7b00891>¶
 Bak, U. G., Nielsen, C. W., Marinho, G. S., Gregersen, Ó., Jónsdóttir, R., & Holdt, S. L. (2019). The seasonal variation in nitrogen, amino acid, protein and nitrogen-to-protein conversion factors of commercially cultivated Faroese *Saccharina latissima*. *Algal Research*, 42, 101576. <https://doi.org/10.1016/j.algal.2019.101576>¶
 Bozzetti, C., El Haddad, I., Salameh, D., Daellenbach, K. R., Fermo, P., Gonzalez, R., Minguillón, M. C., Iinuma, Y., Poulain, L., Elser, M., Müller, E., Slowik, J. G., Jaffrezo, J.-L., Baltensperger, U., Marchand, N., & Prévôt, A. S. H. (2017). Organic aerosol source apportionment by offline-AMS over a full year in Marseille. *Atmospheric Chemistry and Physics*, 17(13), 8247–8268. <https://doi.org/10.5194/acp-17-8247-2017>¶
 Canonaco, F., Crippa, M., Slowik, J. G., Baltensperger, U., & Prévôt, A. S. H. (2013). SoFi, an IGOR-based interface for the efficient use of the generalized multilinear engine (ME-2) for the source apportionment: ME-2 application to aerosol mass spectrometer data. *Atmospheric Measurement Techniques*, 6(12), 3649–3661. <https://doi.org/10.5194/amt-6-3649-2013>¶
 Castillo, M. D., Kinney, P. L., Southerland, V., Arno, C. A., Crawford, K., van Donkelaar, A., Hammer, M., ...